Tribology International 202 (2025) 110361

Contents lists available at ScienceDirect

Tribology International

journal homepage: www.elsevier.com/locate/triboint

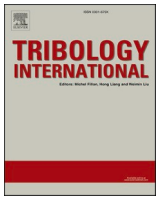

Tribological behaviour of DIN 1.2740 hot working tool steel during mandrel mill stretching process

Hamed Aghajani Derazkola [a,b,c,*], Dieter Fauconnier [c], Ádám Kalácska [c], Eduardo Garcia [a], Alberto Murillo-Marrodán [a], Patrick De Baets [c,d,e]

[a] Department of Mechanics, Design and Industrial Management, University of Deusto, Avda Universidades 24, Bilbao 48007, Spain
[b] Nonlinear Solid Mechanics, Faculty of ET, University of Twente, Drienerlolaan 5, Enschede 7522 NB, the Netherlands
[c] Soete Laboratory, Department of Electromechanical, Systems and Metal Engineering, Ghent University, Technologiepark 46, Zwijnaarde B-9052, Belgium
[d] Flanders Make, The Strategic Research Centre for the Manufacturing Industry, Leuven B-3001, Belgium
[e] Unit of Systems and Component Design, KTH Royal Institute of Technology, Stockholm SE-100 44, Sweden

ARTICLE INFO

Keywords:
DIN 1.2740 hot working tool steel
Pin-on-disk test
Wear
Friction
Surface oxide
High temperature

ABSTRACT

This study evaluates the tribological properties of DIN 1.2740 hot tool steel against Super Cr13 martensitic stainless steel at 700 °C. The results show that the coefficient of friction (COF) ranged from 0.15 to 0.63, indicating moderate frictional interaction. The wear rate of DIN 1.2740 was observed to be low, suggesting good resistance to wear at high temperatures. The complex surface oxide layer that formed on the pin's top surface, significantly reducing the COF and acting as a solid lubricant at elevated temperatures. The oxide layer was also fragile and unable to withstand the high sliding velocities and high loads. The steel exhibited a high surface roughness when subjected to increasing normal loads and increasing sliding velocities.

1. Introduction

Friction and wear are critical factors that can significantly impact industrial manufacturing processes. In certain manufacturing areas, friction can enhance the producibility of a product, while in others, it can lead to defects in the tooling system [1]. The wear and friction effects between the tooling system and workpiece are influenced by factors such as operating temperature, process parameters, applied load, and the strain rate of the process [2]. Among various manufacturing processes, the seamless tube forming process is a complex hot forming process, involving multiple steps to transform a raw billet into a seamless tube. A critical step is the mandrel mill process (MMP). After heating and piercing a billet during skew rolling, the hot pierced workpiece is sized and elongated in MMP [3]. In MMP, a solid mandrel is inserted into the hot pierced billet, and both pass through a sequence of rollers. The number of rollers and the mandrel's length vary according to the desire tube length [4]. During the enlarging and sizing of the hot tube in MMP, the mandrel material experiences high stresses at rapid strain rate in dry conditions (without any lubricant). This situation leads to detrimental wear of the mandrel surface. The mandrel surface wear leads to increased energy consumption and maintenance cost. Understanding the wear and mechanisms gives valuable information for estimating the working life of the mandrel tool and for exploring possible improvement [5]. During MMP, the mandrel plays a crucial role by withstanding various stress components. It serves as a long shaft, maintaining the geometrical accuracy of the elongating tube throughout the process. The mill on its turns transfers the deformation forces from the mandrel to the hot deformable tube. Hence, hard metal like tool steels are commonly chosen for the mill. In most MMP applications, the interface contact between the mill and the hot deformable tube is dry. In such cases, the tribological properties of the mill material becomes vital in order to enhance producibility and reduce energy consumption. However, the available literature lacks comprehensive information on the tribological properties of tool steel under the operating conditions of interest: high temperature, high strain rate, and dry contact. Skela et al. [6] investigated the wear of modified H11-type hot working tool steel between 950 °C - 1150 °C. They found that the wear resistance of this tool is directly linked to chemical and microstructural changes at high temperature. Austenitization at an intermediate temperature of 1030 °C enhances the abrasive wear resistance of the H11 steel under high-stress conditions. Podgornik et al. [7] reported that a low content of Silicon (Si) in AISI H11 tool steel improves its core hardness and wear resistance

* Corresponding author at: Department of Mechanics, Design and Industrial Management, University of Deusto, Avda Universidades 24, Bilbao 48007, Spain.
E-mail address: h.aghajaniderazkola@utwente.nl (H. Aghajani Derazkola).

https://doi.org/10.1016/j.triboint.2024.110361
Received 19 September 2024; Received in revised form 25 October 2024; Accepted 30 October 2024
Available online 4 November 2024

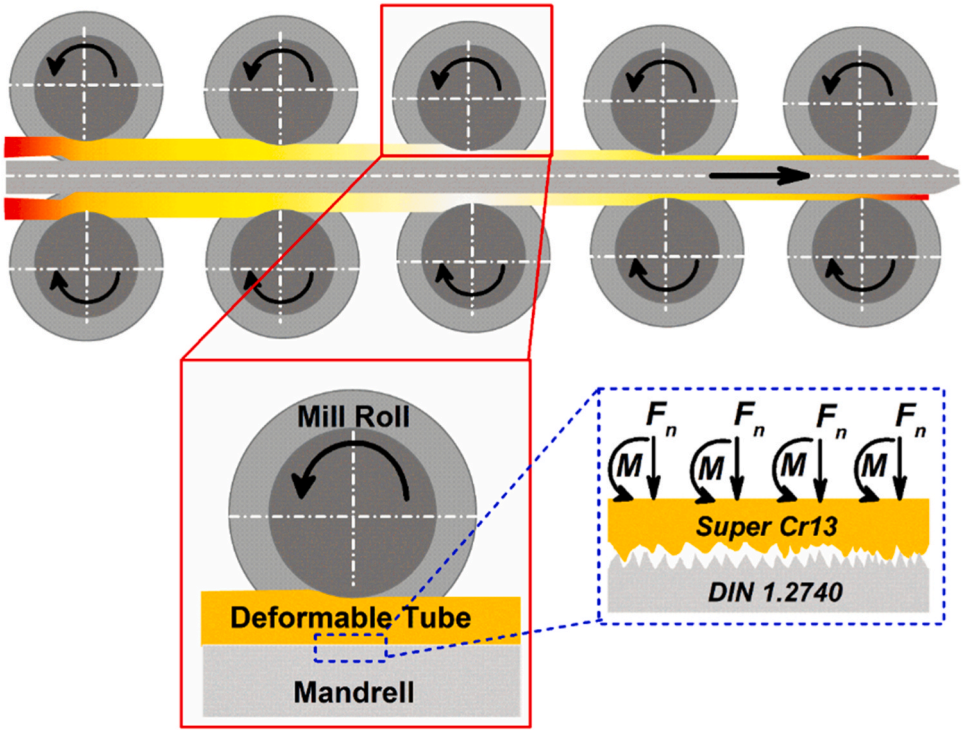

Fig. 1. Schematic view of the MMP of Super Cr13 stainless steel.

Table 1
Chemical composition of test materials.

Super Cr13 martensitic stainless steel											
Element	C	Cr	Ni	Mn	Si	Mo	P	S	Ti	V	Fe
wt%	0.03	11.5–13.5	4.5–6.5	0.5	0.5	1.5–3	0.03	0.005	0.01–0.5	0.5	Bal
DIN 1.2740 (28NiCrMoV10)											
Element	C	Cr	Ni	Mn	Si	Mo	P	S	V		Fe
wt%	0.24–0.32	0.60–0.90	2.30–2.60	0.20–0.40	0.30–0.50	0.50–0.70	0.03	0.03	0.25–0.32		Bal

Table 2
Process parameter used in this study.

Parameter	Unit	Value
Temperature	°C	700
Normal load	N	1, 3, 10
Sliding velocity at R= 20 mm	rpm	500 and 1000
	mm/s	2.1 and 4.2
Sliding distance	m	3000

Table 3
Sample names.

Sample name	Normal Load	Sliding velocity	Sliding distance
Case (I)	1 N	500 rpm	3000 m
Case (II)	1 N	1000 rpm	3000 m
Case (III)	3 N	500 rpm	3000 m
Case (IV)	3 N	1000 rpm	3000 m
Case (V)	10 N	500 rpm	3000 m
Case (VI)	10 N	1000 rpm	3000 m

at high temperatures. Conversely, a high Si content reduces the wear resistance at high temperature. Tian et al. [8] investigated the tribological behaviour of high strength steel Advanced 1500 at high temperature. They reported that both temperature and tribo-test sliding velocity play critical roles in the wear process of this steel. According to their findings, the tribological properties of Advanced 1500 at 500 °C are similar to those at room temperature, but they decrease significantly at 600 °C. On the other hand, at 25 mm/s the main wear mechanism observed was adhesive wear, whereas at 75 mm/s slight grooves were detected on the worn surface. Xianhua et al. [9] studied the wear mechanism of CH-95 against H11 steel at temperatures of 25 °C, 300 °C, 600 °C, 650 °C and 700 °C, with 0.64 m/s sliding velocity. They found that the wear of CH95 and H11 steels are significantly influenced by their mechanical properties at high temperature. At elevated temperatures, applying minimal testing loads already leads to the formation of oxide layers. However, substantial testing loads result in the plastic deformation of the matrix. In these cases, the oxide layer on the worn surface cannot be adequately sustained. CH95 steel's matrix, however, emonstrates superior high-temperature strength, enabling it to effectively support the oxide layer on the worn surface when compared to H11 steel. Wei et al. [10] conducted tribological tests on H21 tool steel against commercial D2 steel at 500 °C. They heat treated the H21 steel at various tempering range (200 °C - 700 °C) to analyse the effects of H21 microstructure on wear mechanism. Their findings indicated that the microstructural variations and plastic deformation of H21 steel lead to the formation of tribo-oxides and increased microstructure stability, enhancing wear resistance.

Many aspects of the tribological properties of tool steels at high temperatures are still not fully understood. The effects of applied stress at high sliding velocity (similar to high strain rate in manufacturing processes), surface chemical changes, and the impact of surface oxide

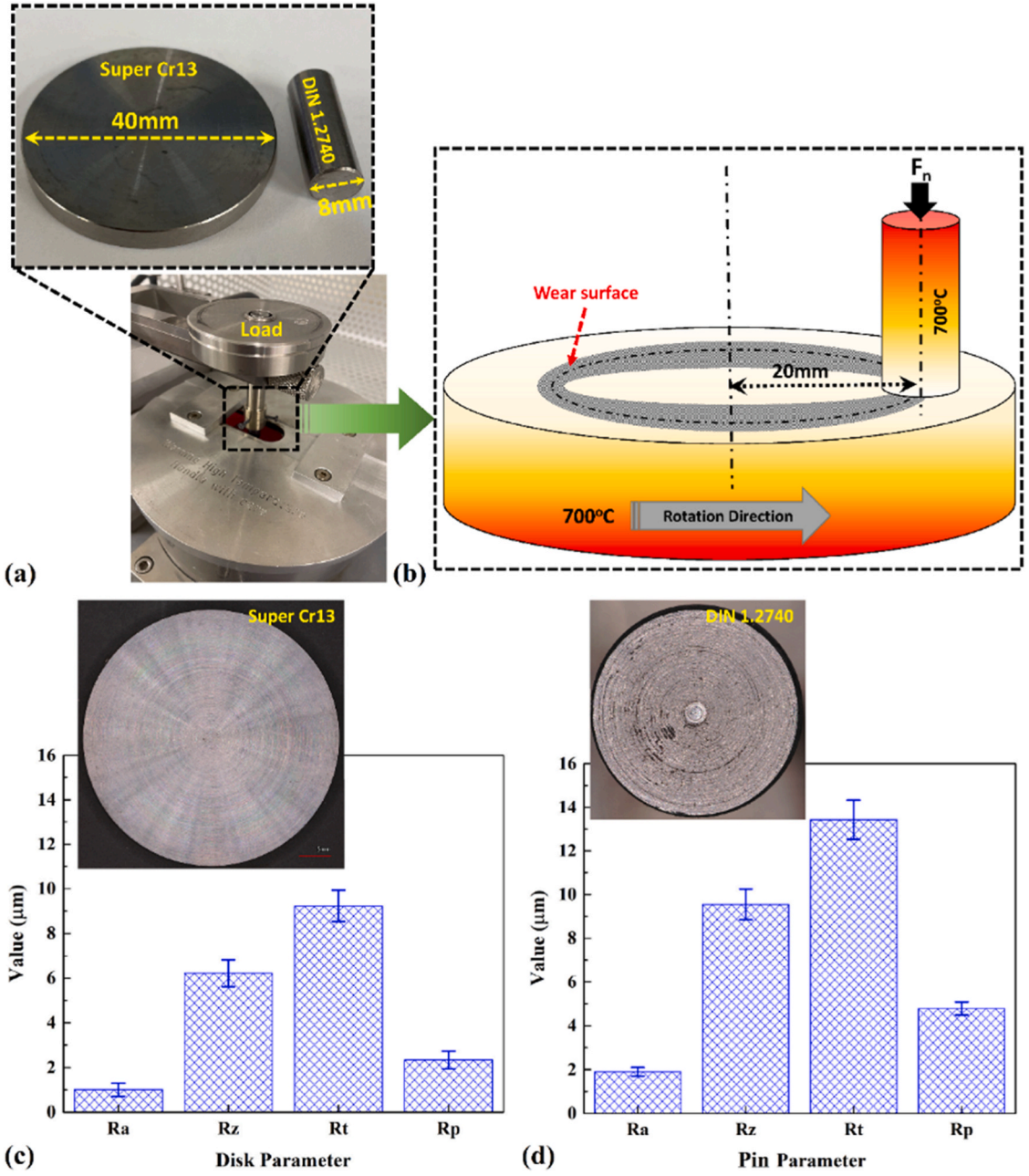

Fig. 2. (a) CSM machine and the dimensions of pin and disk; (b) Schematic view of hot friction test; (c) (d) surface analysis results of Super Cr13 MSS steel disk and DIN 1.2740 disk before testing.

layers on friction are examples of tribological properties that should be examined in detail.

2. Problem definition

Super Cr13 martensitic stainless steel (MSS) tubes are vital components that are widely used in various petrochemical industries because of their corrosion-resistant properties, making them highly demanded for pipeline structures. To produce seamless tubes from Super Cr13 MSS, the billet should be heated. During the production process, Super Cr13 MSS is heated to 1250 °C and undergoes skew piercing and MMP phases. For this reason, the mandrel mill used for MMP of Super Cr13 MSS must be made from hot working tool steel. DIN 1.2740 (28NiCrMoV10) is a specific type of hot working tool steel used as the mandrel material for MMP of Super Cr13 MSS. DIN 1.2740 is a special hot working tool steel with good thermal shock resistance and excellent toughness at high temperature. This steel is nickel alloyed and air-hardened. During MMP, the DIN 1.2740 mandrel remains at ambient temperature (without preheating) and is pushed into the hot Super Cr13 MSS (1250 °C). Subsequently, the DIN 1.2740 mill and hot Super Cr13 MSS become a unified component when they pass through the roller boxes. A schematic view of the MMP process is presented in Fig. 1. In this situation, Super Cr13 MSS acts as a deformable material while DIN 1.2740 mill tolerates a high thermo-mechanical cycle, reducing the thickness of the Super Cr13 MSS. The normal force (F_N) and rolling force moment (M) of the roll mills are transferred to the mandrel, leading to wear of its surface [11].

As mentioned earlier, DIN 1.2740, which is used as a mandrel, falls under the category of hot working tool steel, and its wear during high-temperature operating are very important. The wear of DIN 1.2740 poses a significant issue for Tubos Reunidos, a local company in the north of Spain, as it leads to defects in their mill [11]. The company

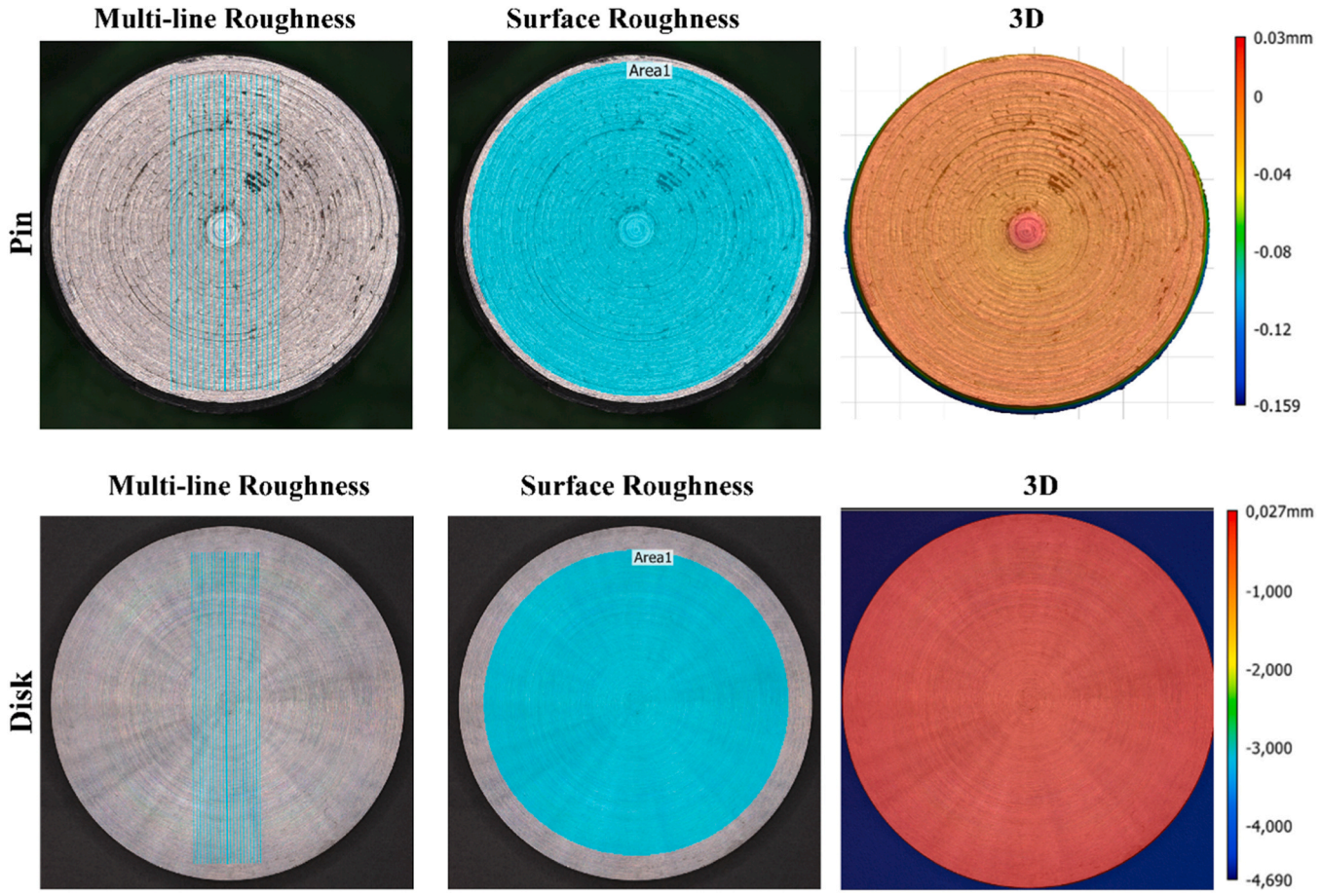

Fig. 3. Surface analysis method of pins and disks.

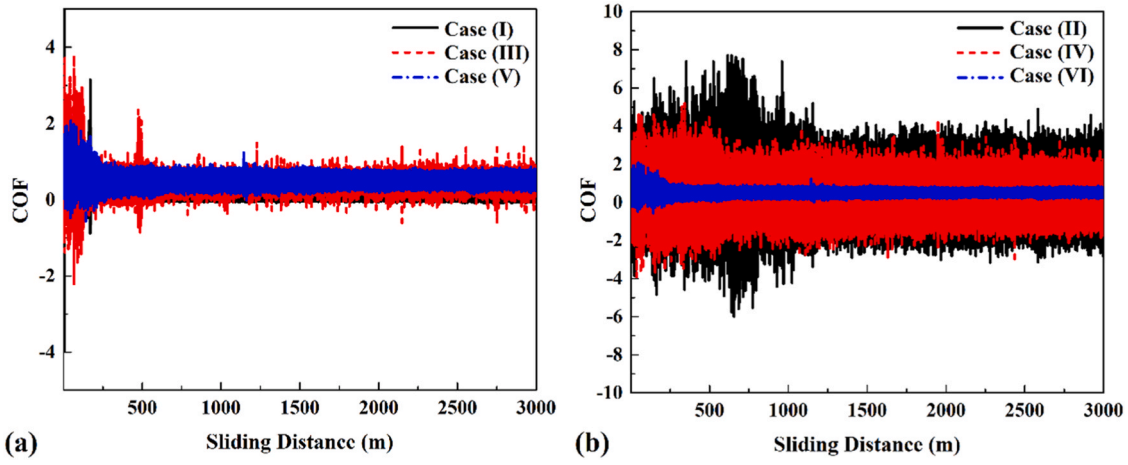

Fig. 4. COF plots in (a) 500 rpm and (b) 1000 rpm sliding velocity.

incurs costs and downtime in replacing and renewing the mills made from DIN 1.2740 steel. Surprisingly, there is no existing study on the effects of high-temperature tribology of DIN 1.2740 in dry condition. To address this gap, we have investigated the impact of various applied loads (tolerated by DIN 1.2740 as a mill) and sliding velocities on the tribological properties of DIN 1.2740. This study also evaluates the effects of thermo-mechanical and thermo-chemical phenomena on the wear and friction properties of this tool steel. The outcomes of this research hold practical significance for real industrial application, particularly for DIN 1.2740 mills, and contribute valuable insights to the scientific community.

3. Experimental procedure

3.1. Test materials

In this study, the test materials represent the actual MMP. The mill is made from DIN 1.2740 (28NiCrMoV10) tool steel, which is in direct contact with Super Cr13 MSS. The tool under analysis is DIN 1.2740, while the Super Cr13 MSS is hot formed. Both materials were provided

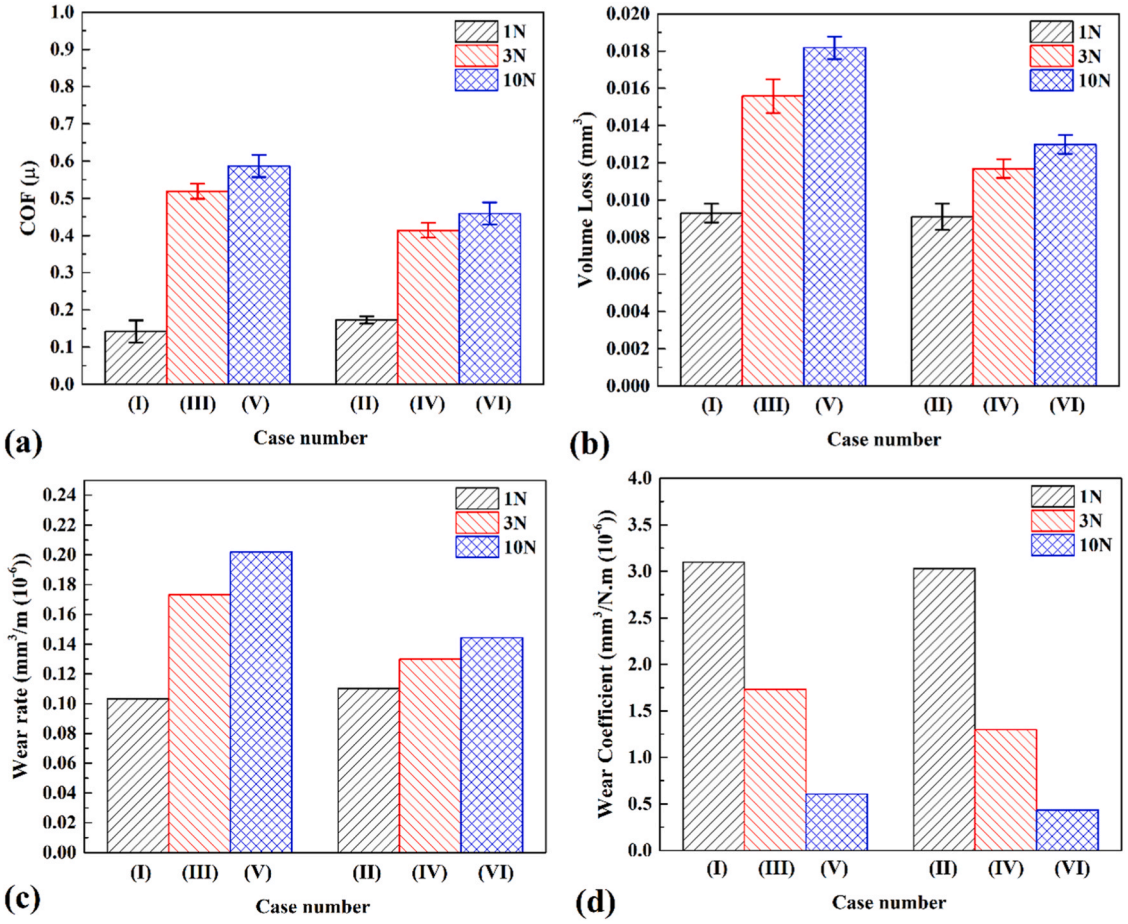

Fig. 5. (a) COF value at various testing conditions; (b) Volume loss; (c) Wear coefficient and (d) Wear rate of DIN 1.2740 pins at various testing conditions.

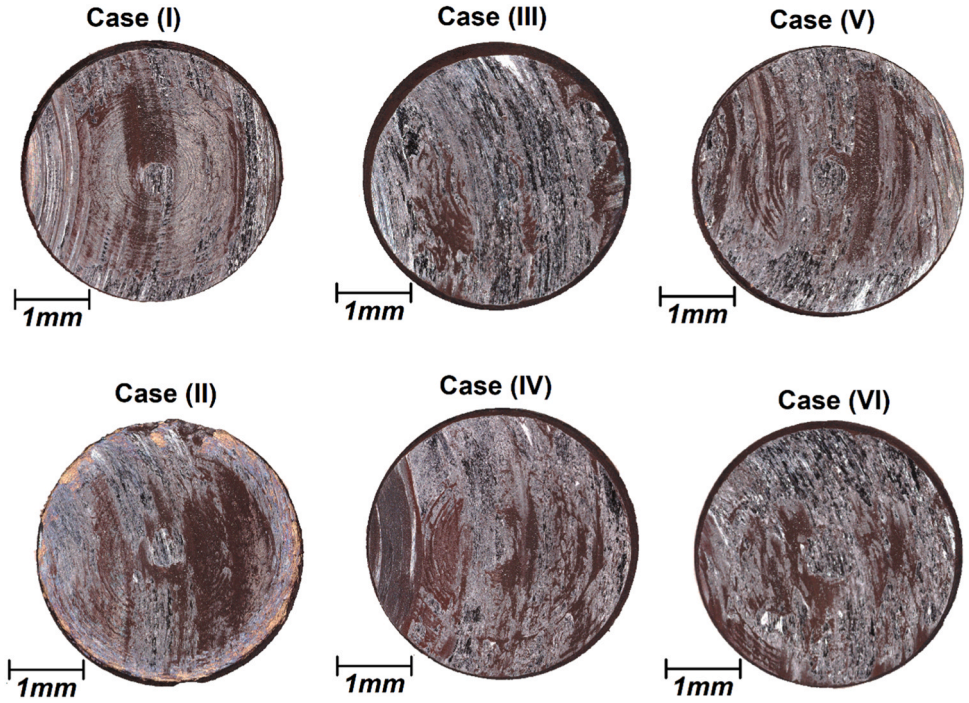

Fig. 6. Optical topography image of pins surface.

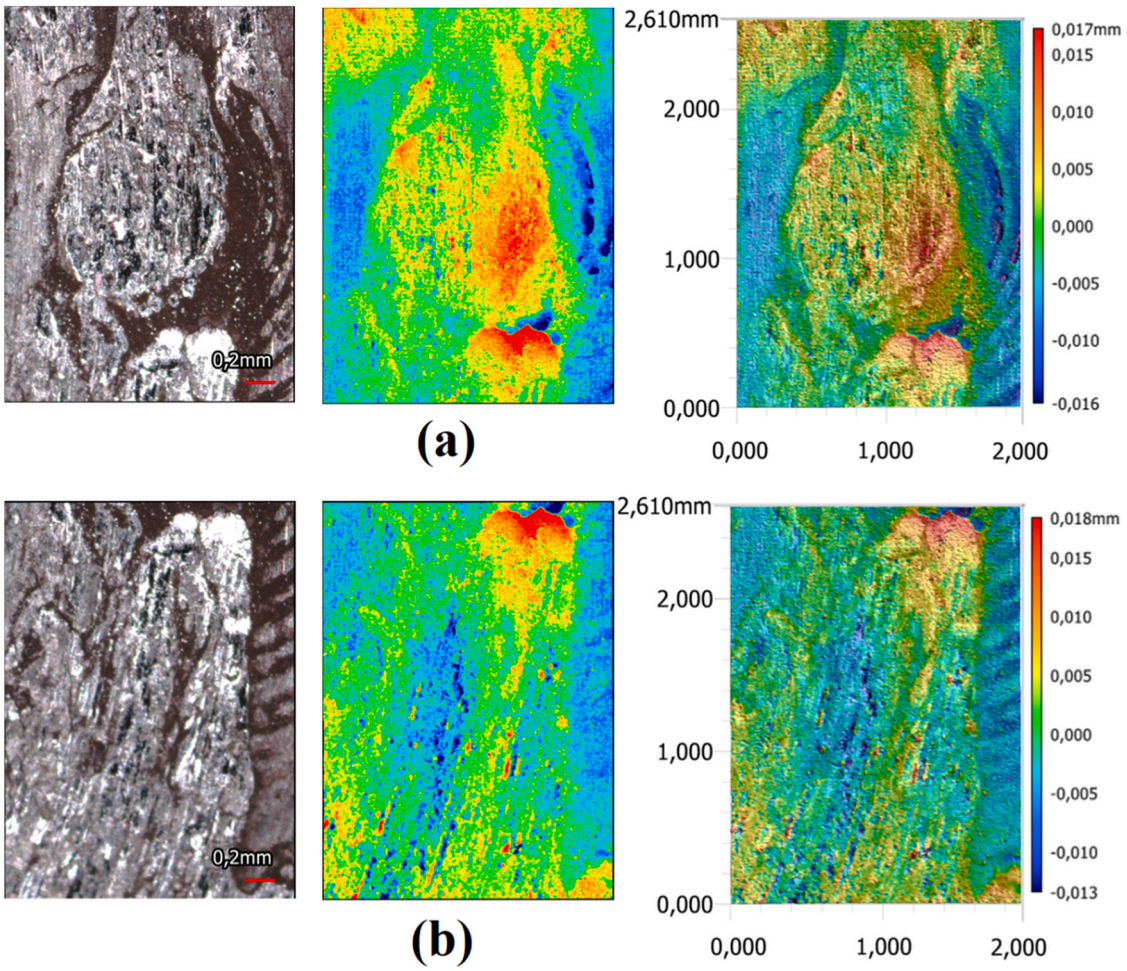

Fig. 7. High magnification surface image of (a) case (III) and (b) Case (IV).

by Tubos Reunidos SA (Madrid, Spain) [11], ensuring identical surface conditions as those found in real MMP. The surfaces of the test materials were machined to match the actual industrial operation. Their chemical composition is detailed in Table 1. The DIN 1.2740 is provided in the form of a cylinder with a diameter of 8 mm and a length of 22 mm. The Super Cr13 MSS is machined into a disk with a diameter of 40 mm and a thickness of 4.5 mm.

3.2. Tribotesting procedure

The testing procedure was designed to replicate the actual temperature and contact condition experienced in the tube manufacturing process. In real manufacturing scenarios, temperature of the deformed tube (Super Cr13 MSS) reaches 1250 °C, while the DIN 1.2740 mill remains at room temperature. In this case, the contact temperature between two components is approximately 700 °C. To simulate these conditions, the tribotesting was conducted using a pin-on-disk test machine (CSM PO/06 high-temperature tribometer, Anton Paar) at around 700 °C. To evaluate the tribological properties of DIN 1.2740, three normal loads and two sliding velocities were chosen. The tests involved a sliding distance of 3000 m. All test conditions were repeated three times, and the average results are presented here. During the test, the pin was positioned perpendicular to the rotational disk, at a radius of 20 mm. Fig. 1a and b depict the test set-up. Table 2 summarizes the testing parameters. For easier reference, the samples were labelled with specific names (see Table 3). The 1 N is chosen to simulate light contact or wear conditions, and increasing three times of normal force (10 N) is based simulates more severe wear conditions. On the other hand, lower loads (1 N) result in lower contact pressure, which might prevent significant plastic deformation and mainly test friction and mild wear. Higher loads (10 N) increase the contact pressure, potentially causing more aggressive wear or material transfer.

3.3. Sample characterization

After the test, the friction data collected and generates statistical data. The surface profile and roughness of the pins is evaluated using white light interferometer (Keyence VR-5200). The surfaces of the test materials (pin and disk) are analysed before testing. The pins and disks are also analysed after testing. The results are presented in Fig. 2c and d, respectively. Surface analysis employs two methods. Initially, a multi-line examination of both pin and disk surfaces is conducted. In this approach, twenty lines are meticulously chosen for the assessment of surface roughness. The surface roughness of both pins and disks is measured, and the outcomes are scrutinized in comparison to the multi-line results. A visual representation of the surface analysis of a raw pin and raw disk is illustrated in Fig. 3. This methodology is systematically applied to all samples. In instances involving tested samples, the surface roughness assessment is specifically performed on the worn surface of the disk.

The worn surface of pins are examined using a scanning electron microscope (SEM), specifically JEOL 7600 SEM, equipped with an Energy-dispersive X-ray spectroscopy (EDS) system. To quantitatively analyse the chemical elements, the X-ray fluorescence (XRF) is employed. The test is conducted under vacuum conditions using the Rigaku NEX GC EDXRF-machine. For the analysis of tribolayers, the pins

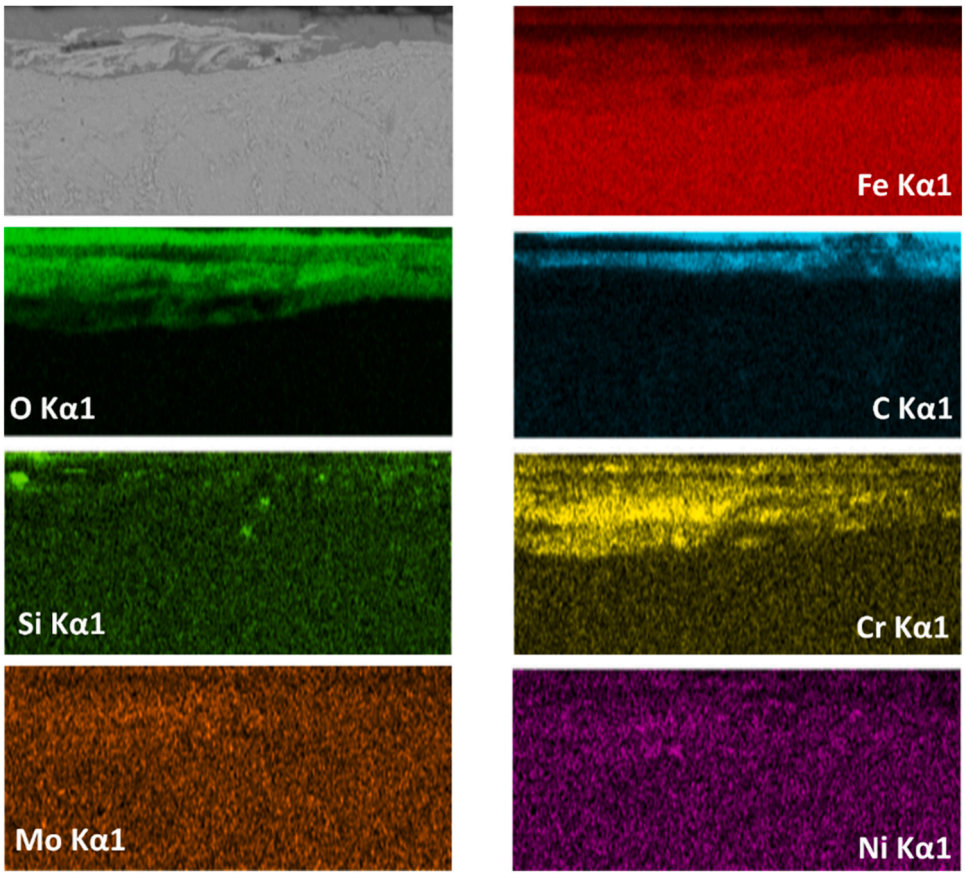

Fig. 8. SEM image and EDS map analysis of sample (I).

are cross-sectionally cut and etched using a 2 % Nital solution. The cross-sections of the pins are examined using optical microscopy (OM).

4. Results and discussions

4.1. Friction and wear analysis

The friction curves during the tests at 500 rpm and 1000 rpm are presented in Fig. 4a and b, respectively. The results show high fluctuations in the early stages of the tests, stabilizing after approximately 100 m. Notably, the COF plot shows more stability at a higher normal load compared to lower normal loads during the test. Additionally, lower sliding velocities show a smoother trend in COF.

The COF values for all cases are presented in Fig. 5a. The results show that the COF of DIN 1.2740 against Super Cr13 MSS is higher at low sliding velocities compared to high sliding velocities. The highest COF is observed at a 10 N load, while the lowest COF is recorded at a 1 N load at both sliding velocities. Specifically, for case (I), case (III), and case (V), the mean COF values are 0.15, 0.51, and 0.63, respectively. Likewise, for case (II), case (IV), and case (VI) the mean COF values are 0.18, 0.42, and 0.49, respectively. The analysis of COF reveals two main perspectives. First, as the normal load increases, the COF between DIN 1.2740 and Super Cr13 MSS also rises. Secondly, sliding velocity affects the COF differently. In contrast to the normal load, increasing sliding velocity reduces the COF at the pin-disk interface. The results show a significant COF difference between 1 N and 3 N, whereas the difference in COF between 3 N and 10 N is relatively minor. Statistical information regarding the volume loss, wear coefficient, and wear rate of DIN 1.2740 is presented in Fig. 5b, c and d, respectively. The data indicates that the wear rate of DIN 1.2740 is relatively mild wear. The volume loss and wear rate of DIN 1.2740 are higher at low sliding velocities compared to high sliding velocities. An increase in normal load amplifies the wear rate of DIN 1.2740. The maximum wear rate occurs at a 10 N load, while the minimum wear rate is recorded at a 1 N normal load.

4.2. Pin Surface morphology

The images displaying the surface of DIN 1.2740 pins after the test are presented in Fig. 6. These images show the pin surfaces after a 3000 m sliding distance. After the test, the surface pre-pattern from the machining process has disappeared. Curvy rings on the surface of all samples are visible. These rings result from the rotational motion of the disk (Super Cr13 MSS) on the pin surfaces.

The pin surfaces exhibit various features such as black zones, white and shiny spots, and dark and faded brown areas. While these colourful areas lack a specific pattern, it can be deduced that the brown area is more prominent in samples subjected to a sliding velocity of 1000 rpm. A high magnification surface analysis was carried out to understand the various colours observed. Surface profilometry images from the centre of case (III) and case (VI) are presented in Fig. 7a and 7b, respectively. The objective is to understand the relationship between physical phenomena and colour paths [12]. Analysis of surface topography images revealed that the white shiny spot areas correspond to the highest peak regions. Dark black and light brown curves correspond to low valleys on the pin surface. The variations in surface topography can be linked to different mechanisms at play during the friction test [13]. The prominent dark black and light brown areas, which are more pronounced at higher normal loads, strongly indicate the occurrence of abrasive wear. With an increase in the normal load, the contact pressure between the pin and the disk intensifies, resulting in greater material removal and the formation of deeper valleys.

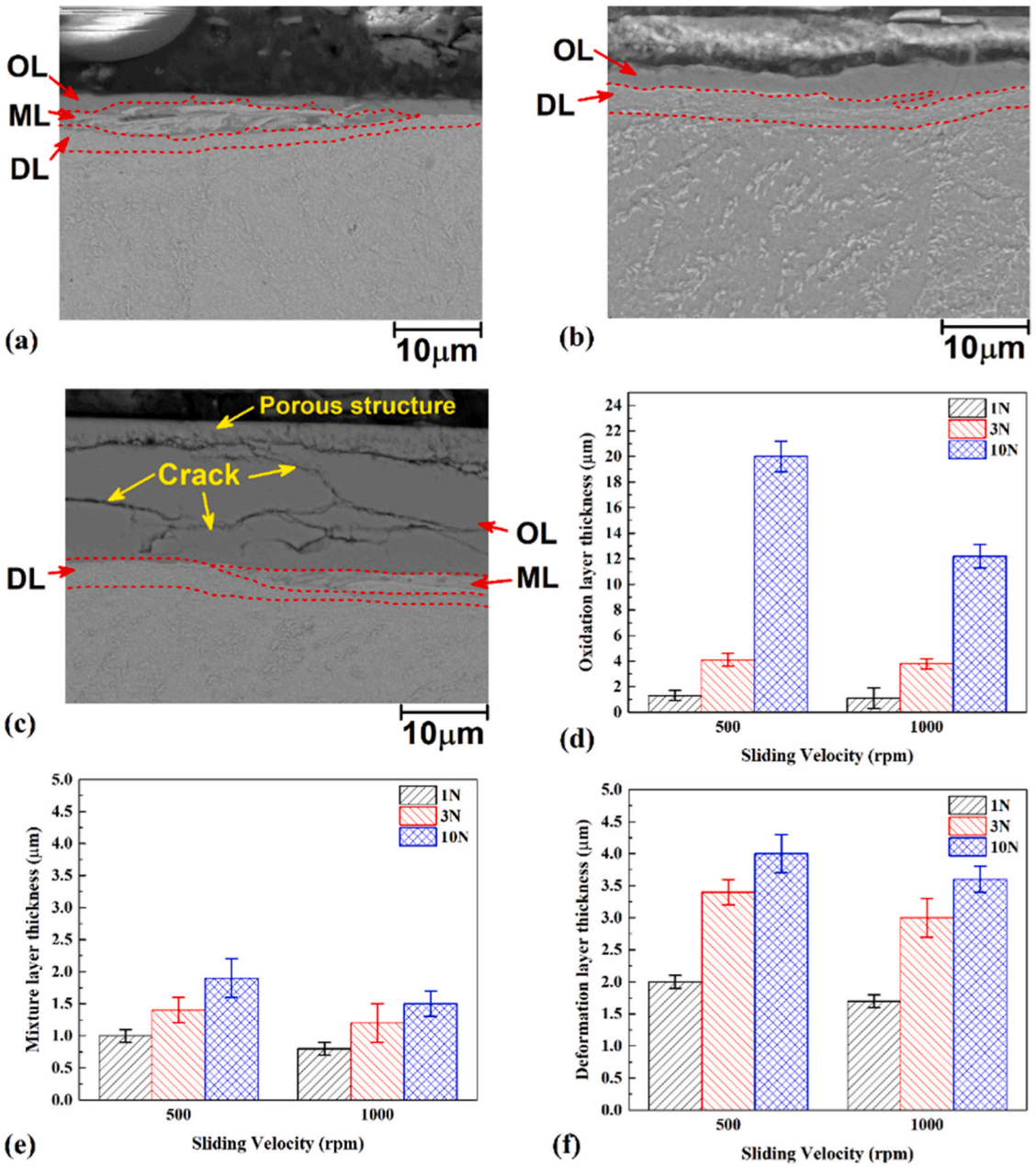

Fig. 9. Cross-section view of (a) Case (I), (b) Case (III), and (c) Case (VI). Average thickness of (d) oxidation layer, (e) mixing layer and (f) deformation layer.

4.3. Pin cross-section

By subjecting a DIN 1.2740 steel to controlled sliding conditions against a Super Cr13 stainless steel rotating disk, the cross-section view of pin provides valuable insights into the tribological behavior. In this case, It is necessary to analyse different chemical phases of pin after tribotest from top to bottom. As a sample, high magnification SEM image and EDS map analysis of Case (I) are presented in Fig. 8. The results shows presence of huge amount of iron oxide at top surface of pin after the test. The EDS map indicated the surface of pins is consists of other elements, which means the chemical composition of pin changes after tribotest. The other elements like carbon (c), Silicon (Si), chromium (Cr), molybdenum (Mo) and nickel (Ni) are exist in pin parent material (DIN 1.2740).

SEM image from a cross-sections of Case (I), Case (III), and Case (VI) are presented in Fig. 9a, b and c, respectively. In the cross-section view of Case (I), a thin oxide layer (OL), a thin mixture layer (ML), and a thin deformation layer (DL) are observed. The mixture layer exhibits a lamellar structure with oxide and deformed layer blend [14]. It is known that during high-temperature sliding wear tests of metals, oxide layers form on opposing surfaces, preventing direct contact between the pure metals. Over time, as tribotesting progresses, these oxide layers tend to crack and detach due to plastic deformation in the subsurface layer, particularly in the softer material. The plastically deformed material accumulates on the surface, oxidizes, and eventually mixes with particles from the harder material, forming a compact composite layer commonly referred to as the 'glaze layer.' The presence of the OL suggests mild oxidation occurring during low normal loads and sliding velocity. Below the oxidation layer, the ML, consisting of a blend of oxide and a deformed layer, indicates a combination of localized plastic deformation and oxidation. This layer may result from the DIN 1.2740 undergoing slight plastic flow and simultaneous exposure to oxidation. The DL beneath the ML suggests limited plastic deformation of the pin material, indicating that the combination of load and sliding velocity is

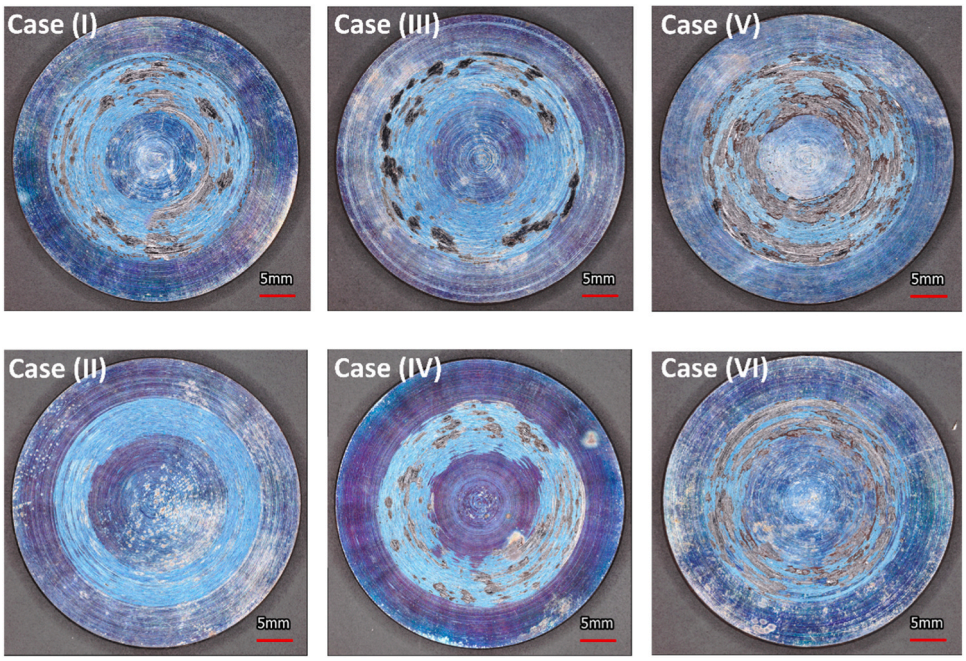

Fig. 10. Optical topography image of disks surface.

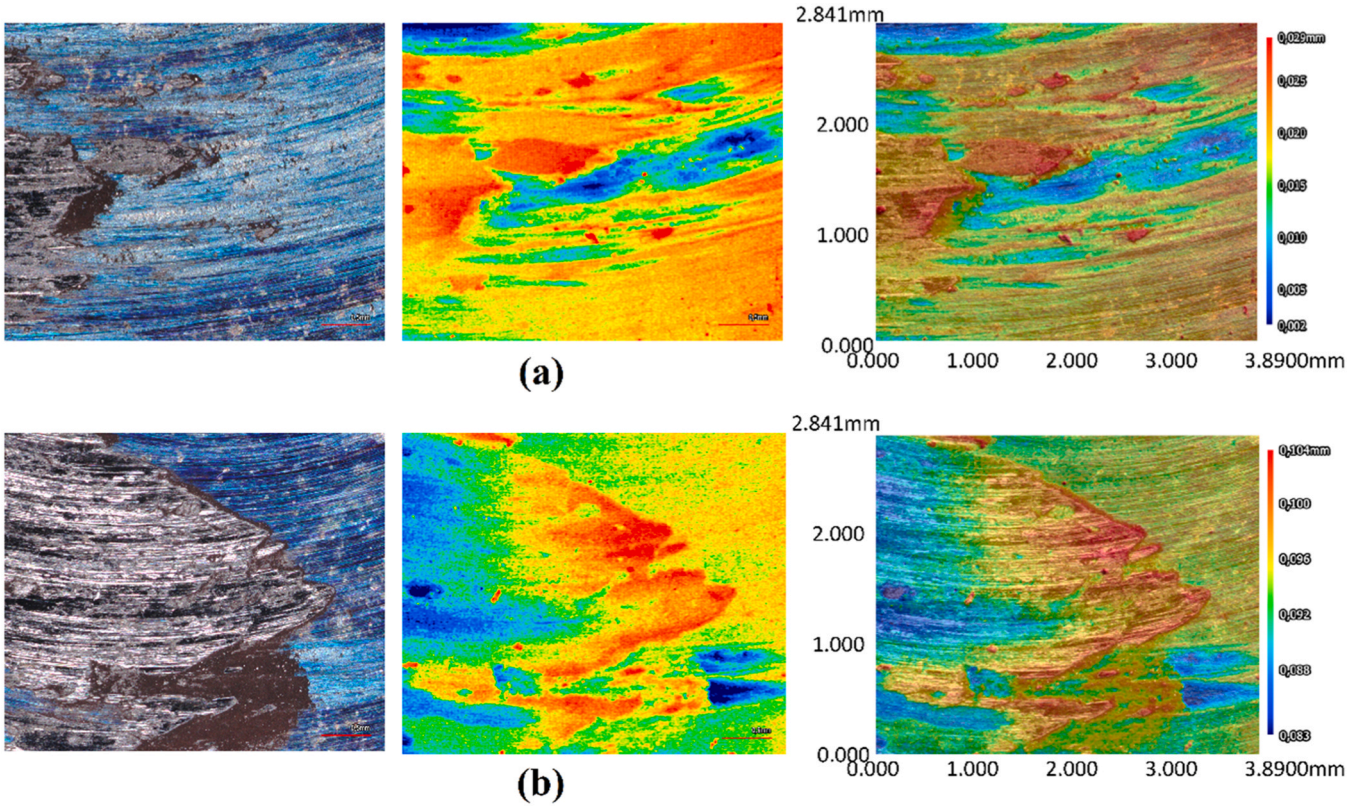

Fig. 11. High magnification disk surface image of (a) case (III) and (b) Case (IV).

insufficient to induce significant plastic flow. This layer-by-layer structure is consistent across all cases.

The cross-section of Case (VI) shows an OL and a DL. The increased thickness of the OL indicates enhanced oxidation due to the higher contact temperatures resulting from the elevated sliding velocity. The thick deformation layer suggests substantial plastic deformation of DIN 1.2740 due to the higher contact pressures and larger frictional forces associated with increased sliding velocity. The combination of higher oxidation and plastic deformation implies that DIN 1.2740 is more prone to wear. In Case (VI), where both low sliding velocity and high normal load are present, the pin's cross-section exhibits a OL, a thin ML, and a thin DL. In this case, the oxide layer is cracked and porous. The thickness of the oxide layer indicates significant oxidation due to the combined effects of low sliding velocity and high normal load. The presence of

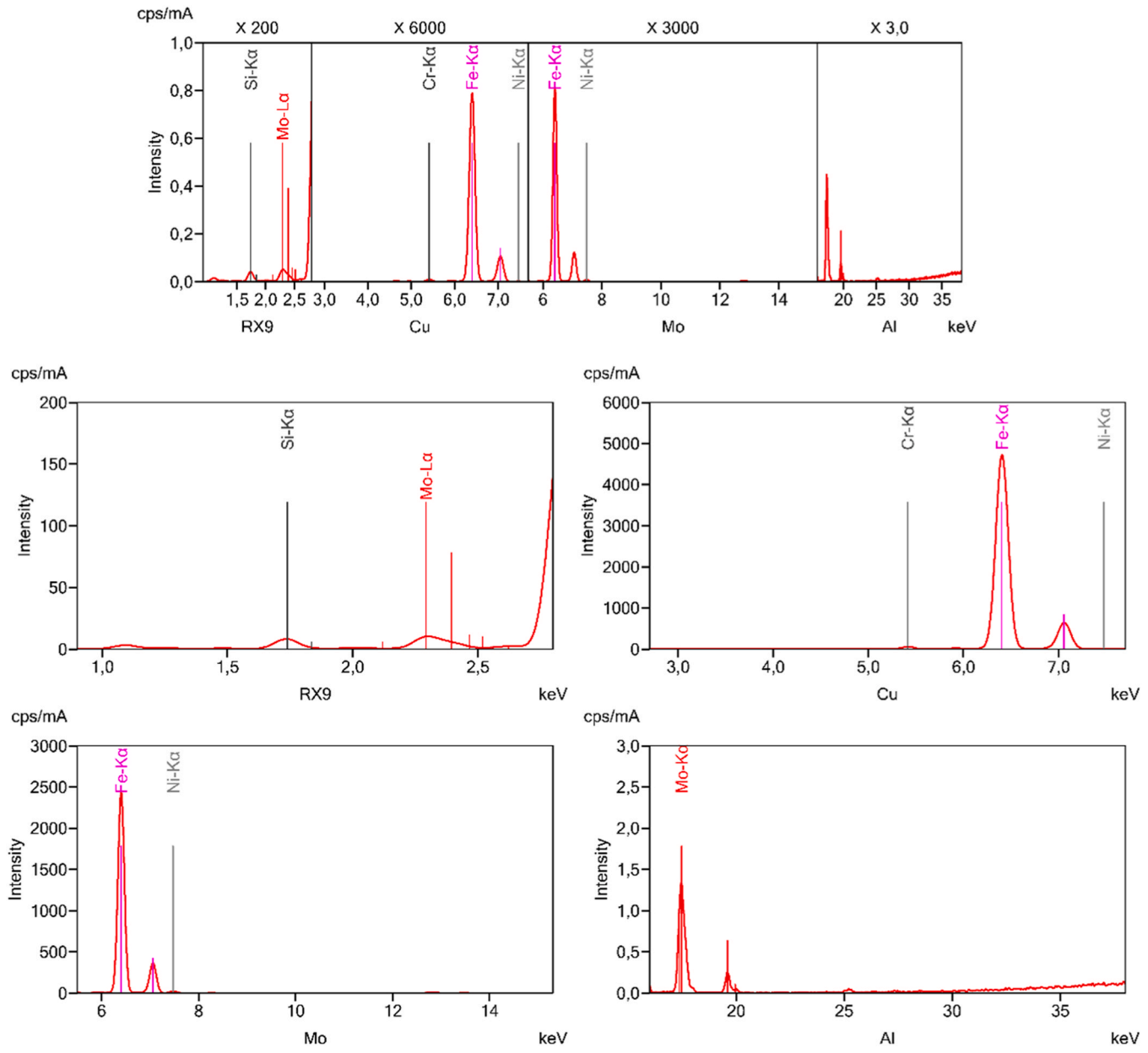

Fig. 12. A sample of XRF analysis results related to the case (III) of pin.

Table 4
XRF results from surface of pins.

	O (mass %)	Fe (mass %)	Si (mass %)	Ni (mass %)	Cr (mass %)	Mo (mass %)
Case (I)	87.3	11.9	0.146	0.111	0.0936	0.0278
Case (II)	86.1	11.1	0.140	0.108	0.0901	0.0259
Case (III)	89.7	9.93	0.166	0.121	0.101	0.0281
Case (IV)	87.6	9.4	0.154	0.119	0.0992	0.0278
Case (V)	91.5	7.94	0.188	0.125	0.122	0.0302
Case (VI)	89.3	7.11	0.182	0.122	0.116	0.0291

cracks and porosity within the oxide layer suggest that the thick OL experiences thermal stress and potentially also thermal fatigue. The ML indicates interaction between plastic deformation and oxidation. The intense deformation caused by the high normal load and low sliding velocity promotes the mixing of the deformed material with the oxide layer [15]. This mixing may alter the surface properties, potentially negatively affecting the tribological behaviour of the DIN 1.2740. The average thickness of the OL, ML, and DL in various samples is evaluated, and presented in Fig. 9d, e and f, respectively. Statistical analysis shows that with increasing normal load, the thickness of all layers increases, whereas with increasing sliding velocity, the thickness of the layers decreases.

4.4. Disk Surface morphology

In Fig. 10, the surface profilometry images of the disks from the hot pin-on-disk friction test reveal distinctive features that warrant thorough scientific analysis. As the temperature of the disks reaches 700 °C,

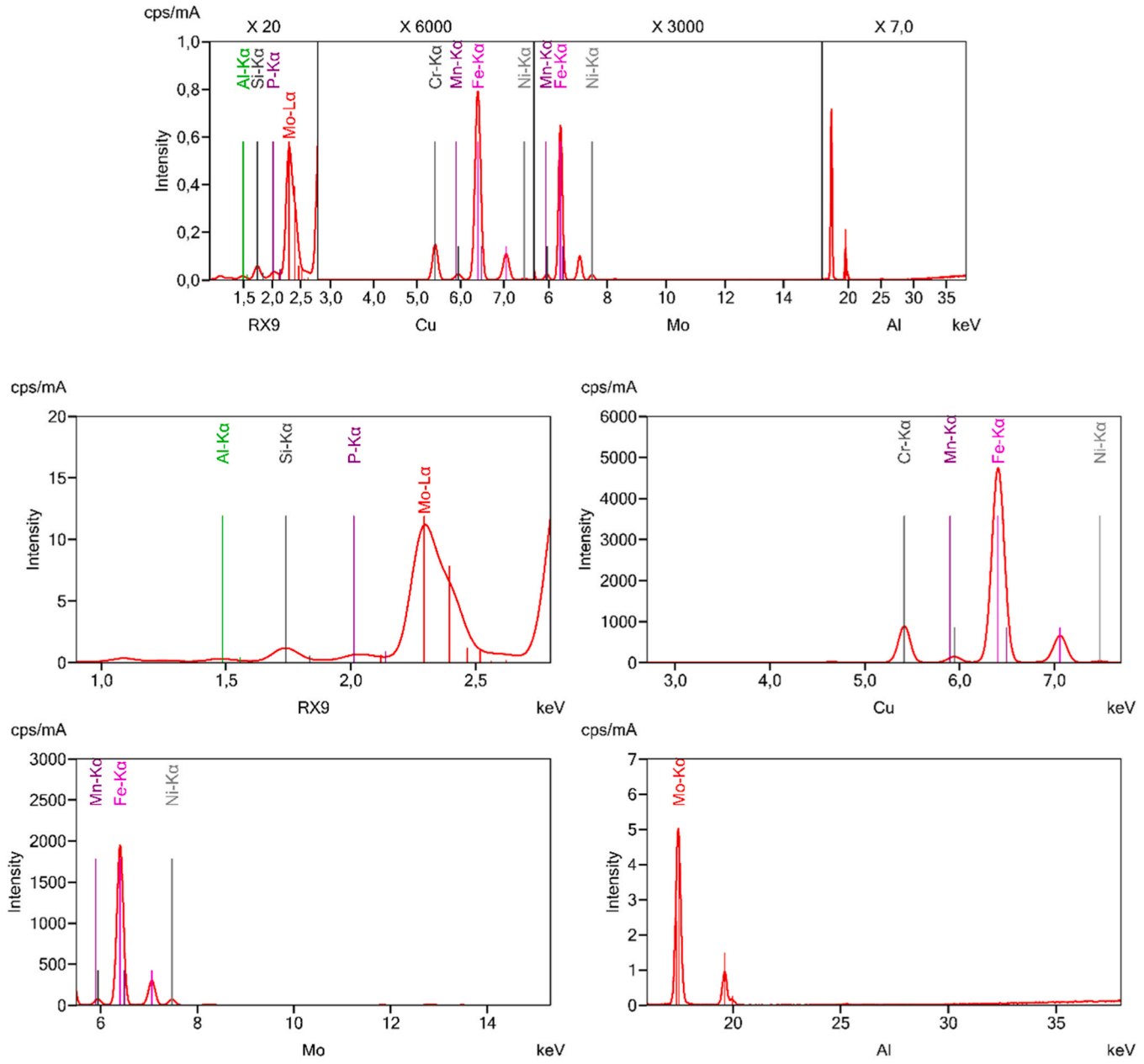

Fig. 13. A sample of XRF analysis results related to the case (III) of disk.

Table 5
XRF results from surface of disks.

	O (mass %)	Fe (mass %)	Si (mass %)	Ni (mass %)	Cr (mass %)	Mo (mass %)	Mn (mass %)
Case (I)	82.2	10.2	0.141	0.111	0.0811	0.0267	0.0012
Case (II)	83.1	10.4	0.137	0.108	0.0779	0.0242	0.0023
Case (III)	87.5	8.73	0.160	0.121	0.0993	0.0267	0.0029
Case (IV)	86.1	8.6	0.148	0.119	0.0932	0.0271	0.0033
Case (V)	90.1	6.61	0.182	0.125	0.115	0.0293	0.0031
Case (VI)	87.1	6.21	0.172	0.122	0.109	0.0287	0.0038

a noticeable change in the color of Super Cr13 stainless steel is observed. This alteration in coloration may be indicative of thermal effects on the material, potentially influencing its mechanical properties during the friction test. The presence of a circular worm area on the disks, which was in direct contact with the pin throughout the test, suggests a localized wear pattern. The circular worm area describes the circular wear track with a worm-like appearance that forms on the disk due to the friction and wear during the pin-on-disk tribotest.

Furthermore, an examination of the overall surface morphology of both the pins and disks highlights the existence of dark and shiny areas on the worn surfaces. The coexistence of these distinct areas signifies variations in the tribological behavior of the materials under different conditions. The dark areas exhibit an increasing trend with higher applied loads, implying a correlation between the magnitude of external force and the extent of material wear. This observation prompts further investigation into the underlying mechanisms governing the frictional response of Super Cr13 stainless steel at elevated temperatures. The surfaces of the disks under investigation display a diverse array of

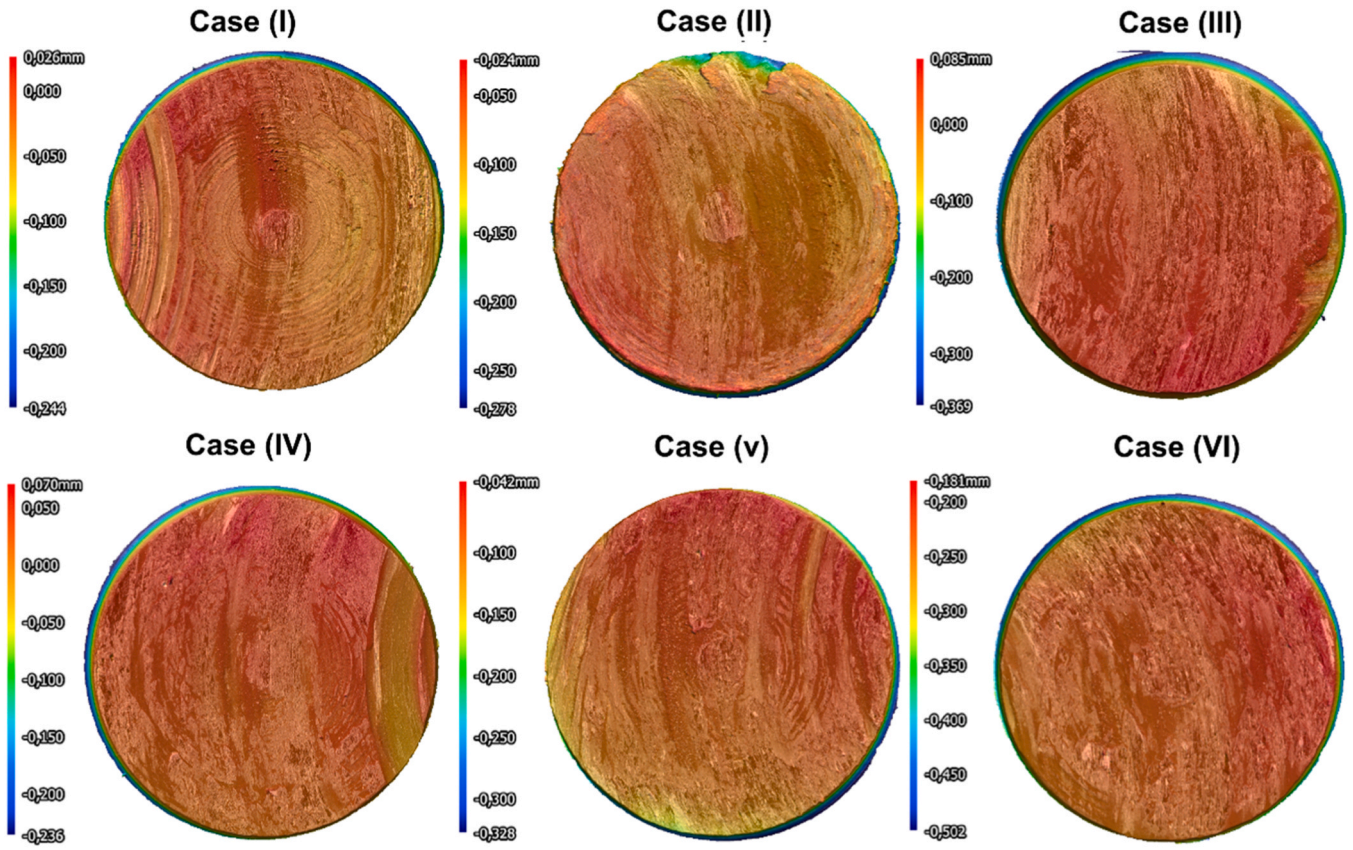

Fig. 14. Surface topography of pins after the tribotest (Zoom and magnification is exactly same as Fig. 6).

features, including black zones, white and shiny traces, and dark and faded brown areas. These distinctive characteristics are not randomly distributed but exhibit stretched patterns along the circumference of the disks-pin contact region. The presence of such patterns suggests a systematic influence, possibly arising from the dynamic interaction between the pin and disk surfaces during the friction test. To delve deeper into the nature of these surface features, a high-magnification surface analysis was undertaken, focusing on specific cases (III and VI). Fig. 11a and b, present surface profilometry images from the center of these cases, offering detailed insights into the topographical variations associated with the observed colors. Upon scrutiny of the surface topography images, a correlation between color and surface elevation becomes evident. The white shiny paths, characterized by their reflective nature, correspond to the highest peak regions on the pin surface. In contrast, the dark black and light brown curves align with low valleys, indicating regions of reduced material height. Additionally, scratched blue areas on the disk surface are identified as moderately worn regions.

4.5. Chemical analysis of surfaces

XRF analysis was conducted on the surface of the pins in order to quantify the chemical composition of the pin surface. XRF result from Case (III) is presented in Fig. 12.

The findings indicate that oxygen, as a major element, and Fe, Ni, Mo, Cr, and Si are the main elements in the surface. The presence of oxygen and iron indicates a significant amount of iron oxide present after the test. The various colours on the pin surface are apparently indicative of iron oxides, visible in different colours compared to the original pin surface. The high testing temperature increased the likelihood of surface oxidations. Additionally, there is a possibility of oxidation during the cooling down of pins after the test. It is important to note that oxygen is a non-fluorescent element, akin to carbon or hydrogen atoms. In this context, the XRF software interprets the observed signal (peak areas or cps) and computes them based on the absorption of fluorescence by oxygen atoms and scattering. Ultimately, the resulting table displays the overall percentage of all surface elements. Consequently, oxygen peaks are not evident in the output graphs [16]. The statistical data regarding oxygen and iron mass percentages at various sliding velocities and normal loads are presented in Table 4. As the testing temperature and environmental conditions were the same across all samples, it is possible to analyse the effects of normal load and sliding velocity on element mass changes at the surface of pins. It is evident that the oxygen mass percentage on the pin surface is higher in samples tested at 500 rpm compared to those tested at 1000 rpm, while the changes in iron mass percentage are less significant. The increased wear rate of DIN 1.2740 at 500 rpm results in higher exposure of fresh hot surface to oxygen, leading to the formation of more oxides either during the test or during the cooling down process.

The presence of dark brown areas, especially at the centre of the pins and particular under higher normal loads, indicates severe oxidation. Accumulation of iron oxide in the centre of the pins contributes to the observed dark brown areas. Thin iron-oxide films have the capability to undergo phase transformations at high temperatures, leading to the formation of a low-friction surface layer [17]. For instance, FeO can transform into a spinel phase, which exhibits good lubricating properties [18]. The lubricating behaviour of thin iron-oxide films at high temperatures can be attributed to several mechanisms [19]. The efficacy of iron-oxide thin films as solid lubricant at high temperatures is influenced by a range of factors, including load, sliding velocity, surface roughness, and environmental conditions [20]. The performance of these films can exhibit substantial variation based on the particular application and operating parameters. In the context of the present study, magnetite demonstrates moderate effects on the COF. In the course of this investigation, a thorough analysis of the disk surfaces has been conducted

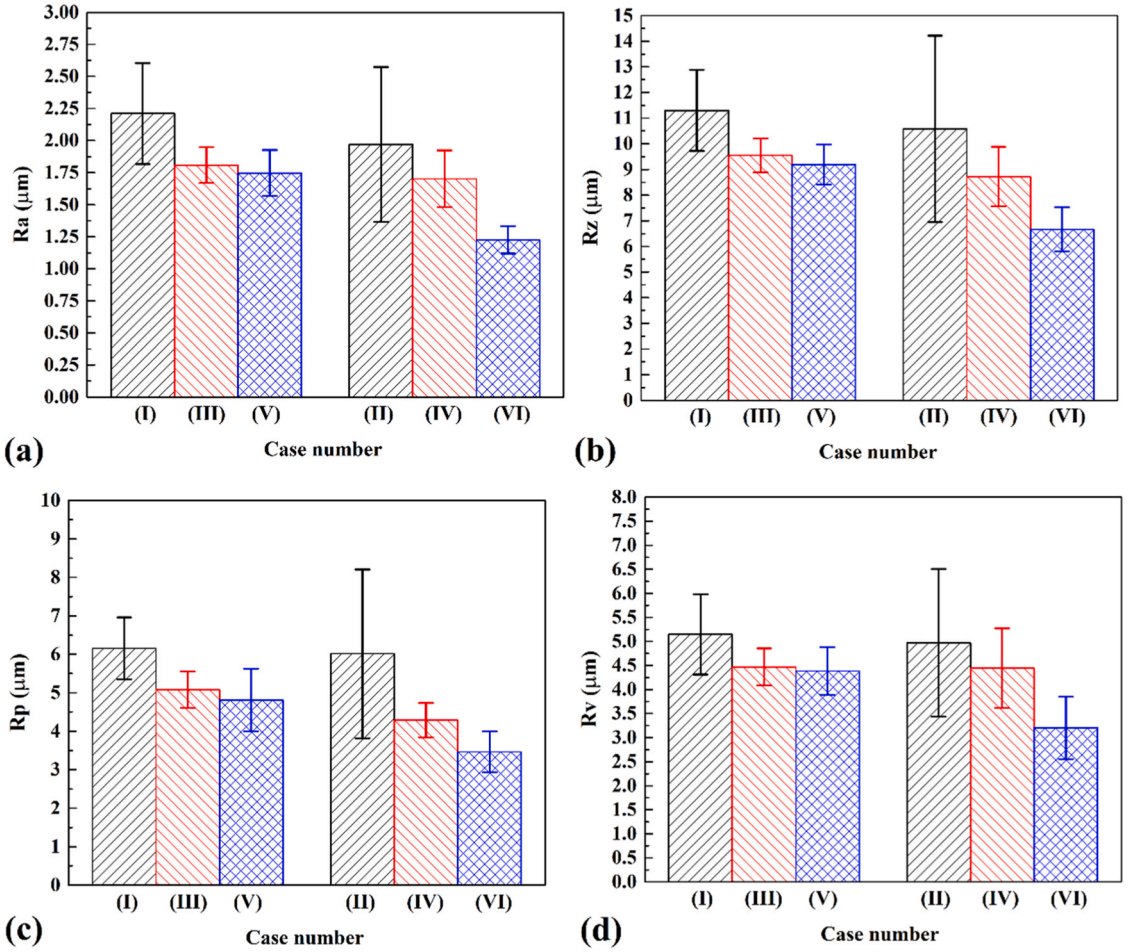

Fig. 15. Statistical results of (a) Ra, (b) Rz, (c) Rp and (d) Rv of pins surface after tribotest.

using XRF, aiming to gain insights into the chemical composition of the surfaces. The findings reveal the presence of elements characteristic of Super Cr 13 stainless steel, accompanied by a noteworthy concentration of oxygen. Fig. 13 illustrates a sample of XRF results specifically from Sample (III), shedding light on the elemental makeup.

Upon closer examination through high-magnification profilometry, it becomes apparent that there is an accumulation of iron oxide concentrated at the center of the worn track. This accumulation contributes significantly to the observed dark brown areas in the detailed profilometry images. This phenomenon aligns with the high levels of oxygen detected on the surface of the disks, mirroring the oxygen-rich composition previously identified on the pin surface. The correlation between the presence of iron oxide and heightened oxygen levels suggests a complex interplay of chemical reactions and wear patterns on the surfaces of both the pin and the disks. The findings of the X-ray Fluorescence analysis for the disk surfaces are comprehensively outlined in Table 5. The outcomes reveal the predominant composition of super Cr13 steel main elements, accompanied by a substantial abundance of oxygen on the disk surfaces. A noteworthy correlation emerges between the alterations in the mass of elements on the disks and corresponding changes observed in the pins. Specifically, as the normal load applied during the test increases, there is a concurrent escalation in the presence of oxygen. The examination of disk images further highlights significant color variations, particularly in the oxide area, concentrated within the contact zone influenced by the pin. This prompts speculation regarding the potential transfer of surface oxide from the pin to the disk. The intricate interplay of elemental composition and observed changes underscores the dynamic nature of surface interactions during the test.

4.6. Surface roughness analysis

The surface roughness of pins after the test are evaluated by optical profilometry. The results for each case are presented in Fig. 14. Due According to obtained results, the surface consists of peak and valley areas. These results indicated that the roughness of pins is not the same in all conditions. The sliding velocity and the applied load can affect the surface roughness of pins.

Both sliding velocity and normal load exert significant influence on the surface roughness of the pins. To conduct a thorough analysis of the pins' roughness after the test, several parameters including arithmetical mean height (Ra), maximum height (Rz), highest peak (Rp), and lowest valley (Rv) are measured and depicted in Fig. 15a, 15b, 15c and 15d, respectively. Starting with Ra, the results show that the value of Ra at 500 rpm is higher than at 1000 rpm. Pins subjected to a 1 N normal load exhibit higher Ra values (indicating rougher surfaces) compared to those tested with a 10 N normal load. Specifically, at 500 rpm sliding velocity, Case (I) has the highest Ra value of 2.23 μm, Case (II) has an intermediate Ra value of 1.82 μm, and Case (V) exhibits the smoothest surface with a Ra value of 1.74 μm. Under the condition of 1000 rpm sliding velocity, Case (II) has the highest Ra value of 1.95 μm, Case (IV) has an intermediate Ra value of 1.63 μm, and Case (VI) shows the smoothest surface with a Ra value of 1.17 μm. These results align with the established understanding that higher Ra values correspond to increased surface roughness, resulting from elevated friction, wear, and material loss.

Regarding the Rz parameter, which measures the maximum peak-to-valley height, it follows the same trend as Ra. Among the tested conditions, Case (I) exhibits the highest value of 11.3 μm, and Case (VI) shows

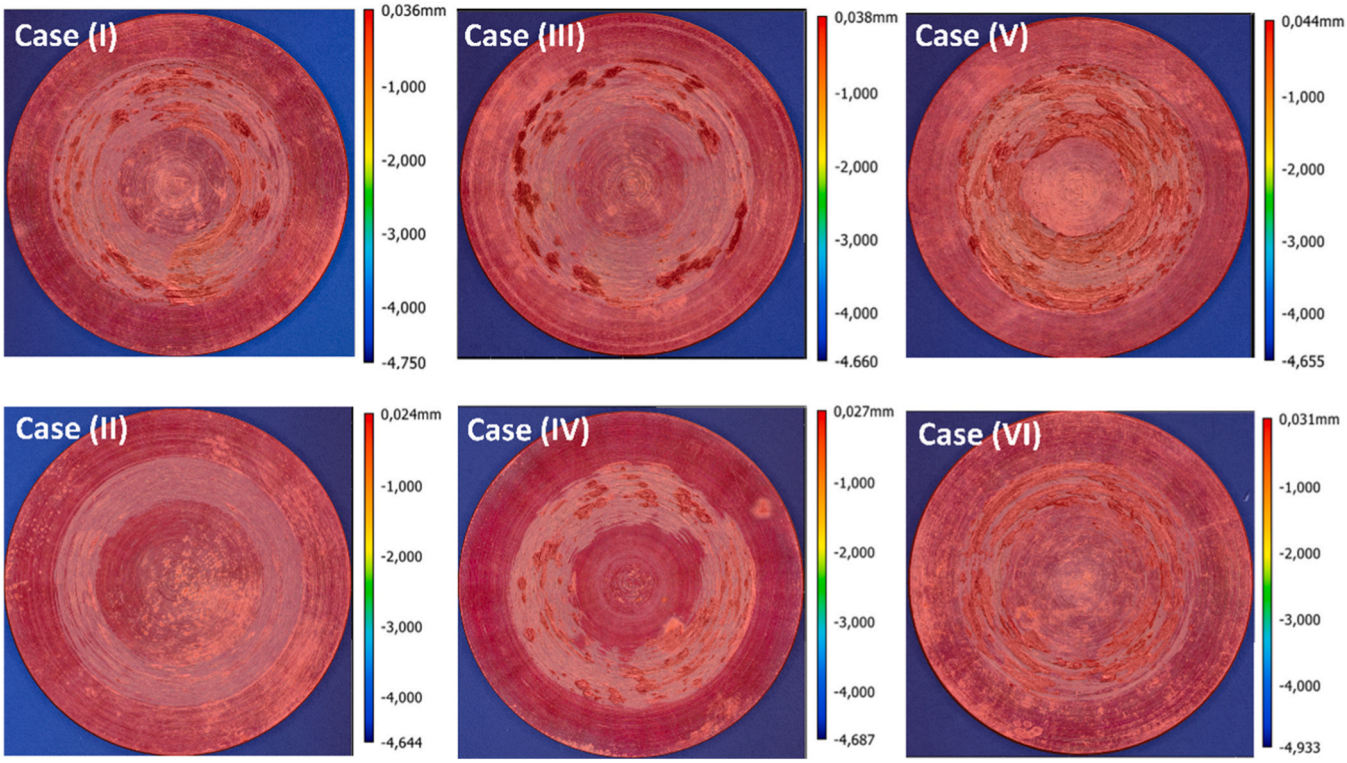

Fig. 16. Surface topography of disks after the tribotest (Zoom and magnification is exactly same as Fig. 10).

the lowest value with an Rz of 6.4 μm. These results indicate that Case (I) has the most substantial surface irregularities, indicating more significant wear and lower deformation compared to the other samples. Considering the Rp and Rv parameters, which measure the maximum peak height and valley depth, DIN 1.2740 pins followed the same trend as Ra and Rz. Highest values of Rp (6.1 μm) and Rv (5.2 μm) belong to case (I) and the lowest values of Rp (5.1 μm) and Rv (3.2 μm) belong to case (VI). The Rp parameter provides insights into the highest peaks on the surface, which can be associated with localized wear or damage. Therefore, it can be inferred that Case (I) experienced the most significant localized wear, while Case (VI) had the least. From the above we can conclude that Case (I) consistently displays the highest values across all parameters, indicating the roughest surface, the largest amplitude of surface irregularities. In contrast, Case (VI) consistently demonstrates the lowest values, indicating the smoothest surface. From a wear perspective, these results imply that Case (I) likely experienced the most severe wear due to its high surface roughness and significant amplitude of surface irregularities. On the other hand, Case (VI)'s smoother surface and lower roughness parameters indicate better resistance to wear and deformation. The surface roughness of disks after the test are evaluated by optical profilometry. The results for each case are presented in Fig. 16.

In this tribotest, surface parameters of the disks were examined, as illustrated in Fig. 17. The analysis of Ra, Rz, Rp, and Rv, presented in Fig. 17a, b, c, and d, respectively, revealed a noteworthy trend. It was observed that the results for the disks exhibited an inverse relationship with those of the pins.

The recorded data indicated that Case (I) yielded the lowest values for Ra, Rz, Rp, and Rv, while Case (VI) exhibited the highest values across all surface parameters. Specifically, the maximum Ra was documented at 1.75 μm in Case (VI), contrasting with the minimum Ra of 0.7 μm in Case (I). Furthermore, Case (VI) displayed the highest Rz at 7.4 μm, whereas Case (I) registered the lowest Rz at 3.5 μm. Additionally, the maximum Rp and Rv were both recorded in Case (VI) at 3.74 μm and 3.8 μm, respectively, while the minimum Rp and Rv were noted in Case (I) at 1.75 μm and 1.6 μm. The variations in surface parameters, such as Ra, Rz, Rp, and Rv, underscore the significance of different testing conditions. The observed differences between pin and disk materials could be attributed to factors such as material properties or contact pressures. The results show an inverse relationship between the surface roughness of the pins and disks. For instance, when the pin exhibits higher surface roughness values (such as in Case (I)), the corresponding disk surface shows lower roughness parameters. This could be due to the higher material transfer from the pin to the disk, smoothing out the disk surface while leaving the pin with more pronounced wear and surface irregularities. In contrast, in Case (VI), where the pin demonstrates lower roughness, the disk shows higher roughness values. This suggests less aggressive wear on the pin and more material accumulation or surface damage on the disk, leading to a rougher disk surface.

4.7. Wear mechanism of Pin

As mentioned earlier, the surface of pins exhibited various thermo-mechanical phenomena, such as surface deformation and surface oxidation, during the test. These surface changes on the pin were not uniform, occurred locally and were influenced by the test parameters. The SEM image from the surface of the pin in Case (I) after the test is presented in Fig. 18a. The EDS analysis of this pin surface (Fig. 18b) indicates the presence of various elements, primarily from DIN 1.2740 chemical composition, along with oxygen (Fig. 18c). The EDS results show important oxide presence on the pin surface after the test. However, the distribution of elements, even oxygen, is not uniform. This behaviour is observed in almost all other samples as well.

For the wear mechanism analysis, the pin surfaces were examined using SEM after tribotests at different sliding velocities and normal loads. The SEM images in Fig. 19a and 19b present the secondary electrons (SE) image and backscattered electrons (BSE) image of Case (I) and Case (II) surface, respectively. The results reveal scratching, abrasive wear, and deformation of oxidation layers on the pin's surface.

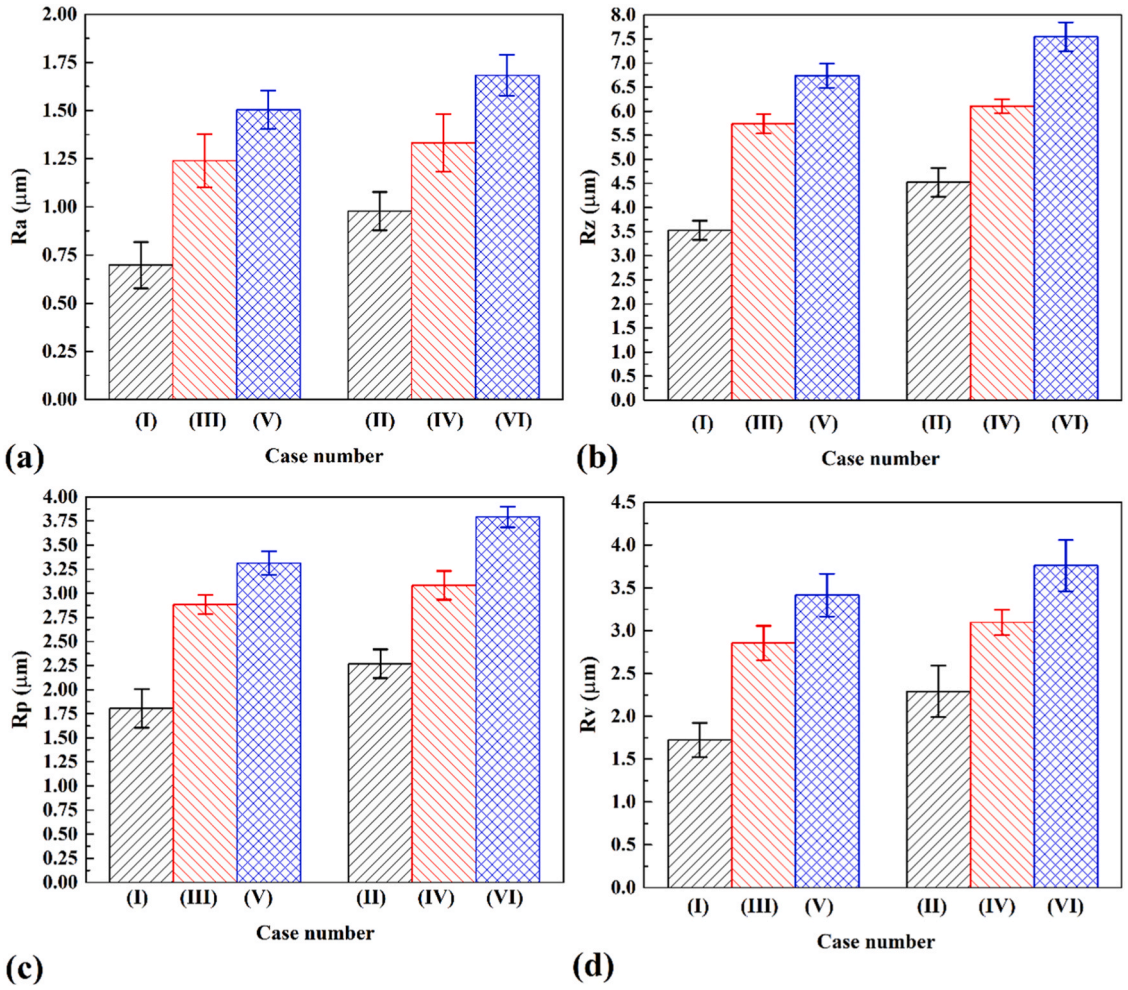

Fig. 17. Statistical results of (a) Ra, (b) Rz, (c) Rp and (d) Rv of disks surface after tribotest.

Abrasive wear indicates that the contact between the pin (DIN 1.2740) and the disk (Super Cr13 MSS) led to material removal and surface damage [21]. The results indicate that at low normal loads and low sliding velocities, abrasive wear is particularly intense in Case (I). At low sliding velocities, abrasive wear can occur due to the presence of hard particles or asperities on the sliding surfaces. These hard particles can cause abrasion, leading to the generation of small debris on the tool steel surface. As a result, abrasive wear became more prominent, leading to severe surface damage [22]. The SEM analysis reveals the presence of oxidation layers (OL) as small islands on the surface of Case (II) that presents in Fig. 19b. These layers were detected in tests conducted at low normal loads and high sliding velocities. The oxidation layers acted as protectors, reducing the abrasive wear observed on the surface. However, it was also observed that the oxidation layer can deform, scratch, and detach under high normal loads and low sliding velocities, indicating that the protective capabilities have their limits. The bonding between the oxide layer and the pin surface may not be strong enough to withstand extreme mechanical stresses, leading to localized abrasive wear.

With an increase in normal load, the wear behaviour of the DIN 1.2740 pin underwent some changes. SEM image from the surfaces of Case (V) and Case (VI) are presented in Fig. 20a and b, respectively. As discussed, thicker oxide layers are formed on the surface of Case (V) and Case (IV) compared to other cases. Deformation and abrasive wear were observed on the oxide layer at high normal loads. Furthermore, under high normal load conditions, the oxidation layer covered a larger area on the pin's surface, indicating a more extensive tribo-chemical reaction. However, the bonding between the oxide layers and the pin surface was not strong enough to withstand the high normal load at low sliding velocity (Case (V)), leading to detachment of the oxide layers and localized abrasive wear.

Scratching and abrasive wear in all samples confirm the harsh conditions experienced during the hot friction test. However, the existence of substantial oxidation layers altered the tribological behaviour of the pin. In this specific case, it can be seen that the oxidation layers acted as protective barriers, reducing abrasive wear [23]. Nevertheless, at high normal loads and low sliding velocities, the bonding between the oxide layers and the pin surface proved insufficient to withstand the mechanical stress, resulting in localized abrasive wear. The growth of oxidation layers during the hot friction test suggests a complex interplay between temperature, sliding velocity, and tribo-chemical reactions [24]. During a hot pin-on-disk test on steel, surface intermixing areas can form due to various tribological processes and interactions between the pin and the disk. These intermixing areas consist of particles that are a mixture of surface oxides, particles from the pin material, and particles from the disk material. The formation of such areas can be attributed to tribological phenomena like frictional heating and mechanical mixing. The SEM image from the intermixed area in Case (V) and Case (VI) are presented in Fig. 21a and b, respectively.

Severe deformation and fragmentation of surface oxides (on the pin and disk materials) can be entrained in the contact region and mixed, contributing to intermixed areas. The EDS point analysis of points 1, 2, and 3 indicates the presence of DIN 1.2740 alloy with carbon and oxygen (Fig. 21c). This suggests that the intermixing areas contain a

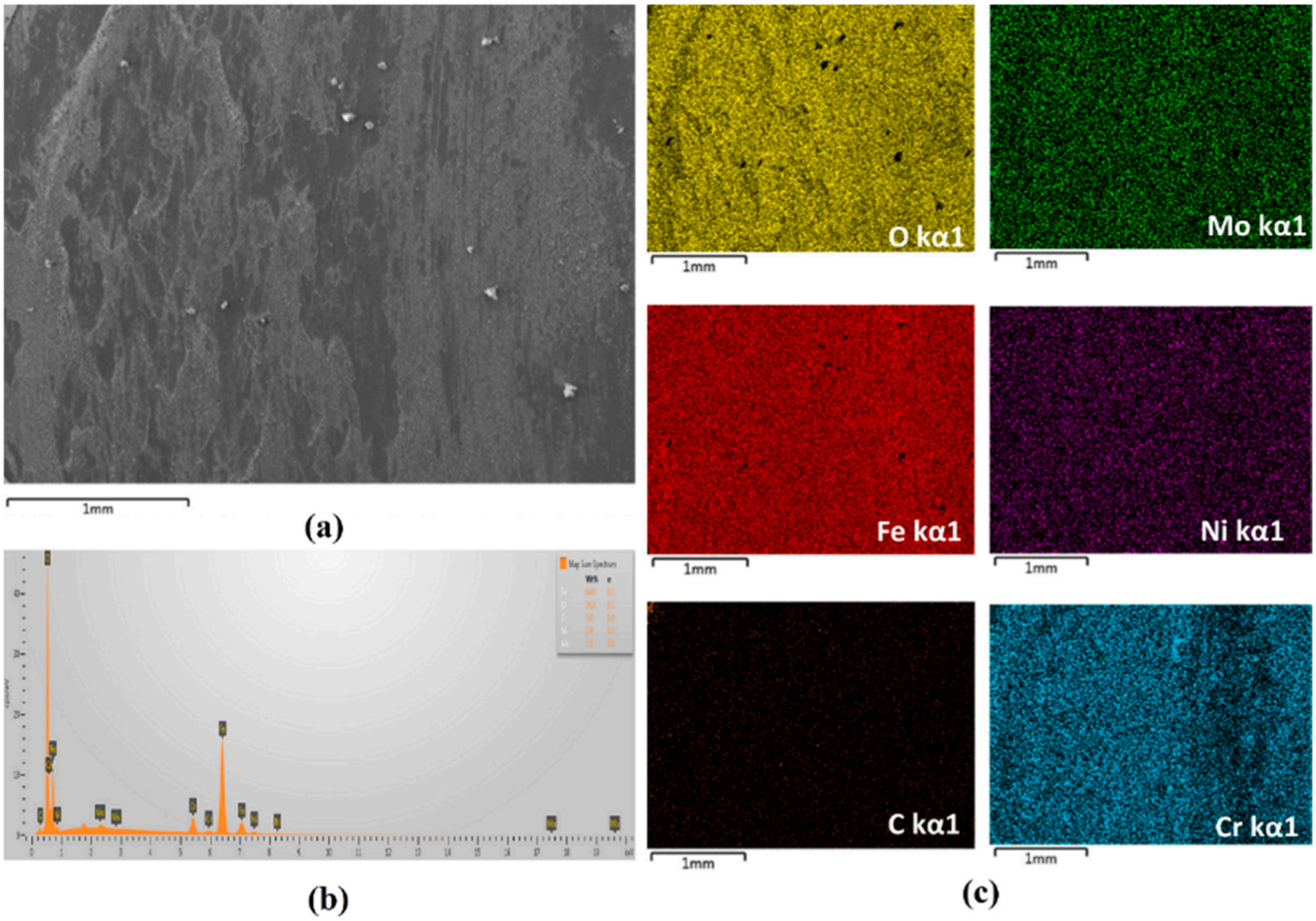

Fig. 18. Low magnification SEM image from surface of the pin in Case (I). (b) EDS analysis and (c) element mapping of Case (I) pin's surface.

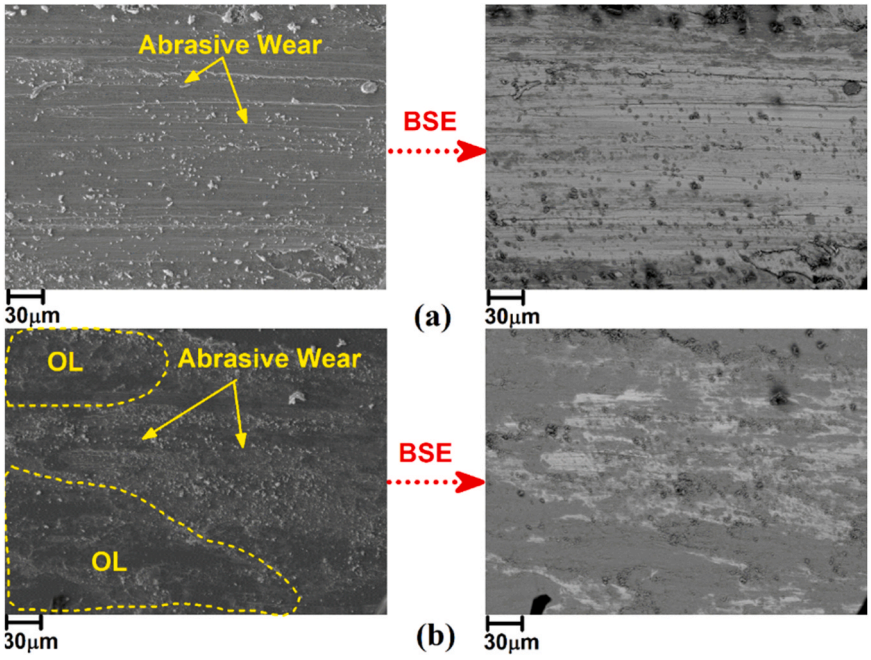

Fig. 19. SE and BSE images from surface of (a) Case (I) and (b) Case (II).

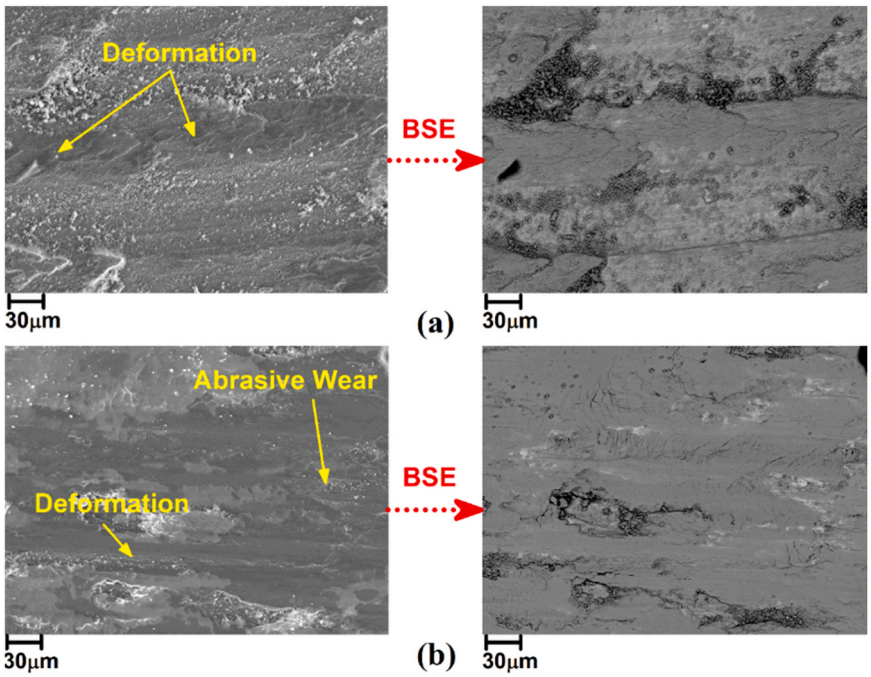

Fig. 20. SE and BSE images from surface of (a) Case (V) and (b) Case (VI).

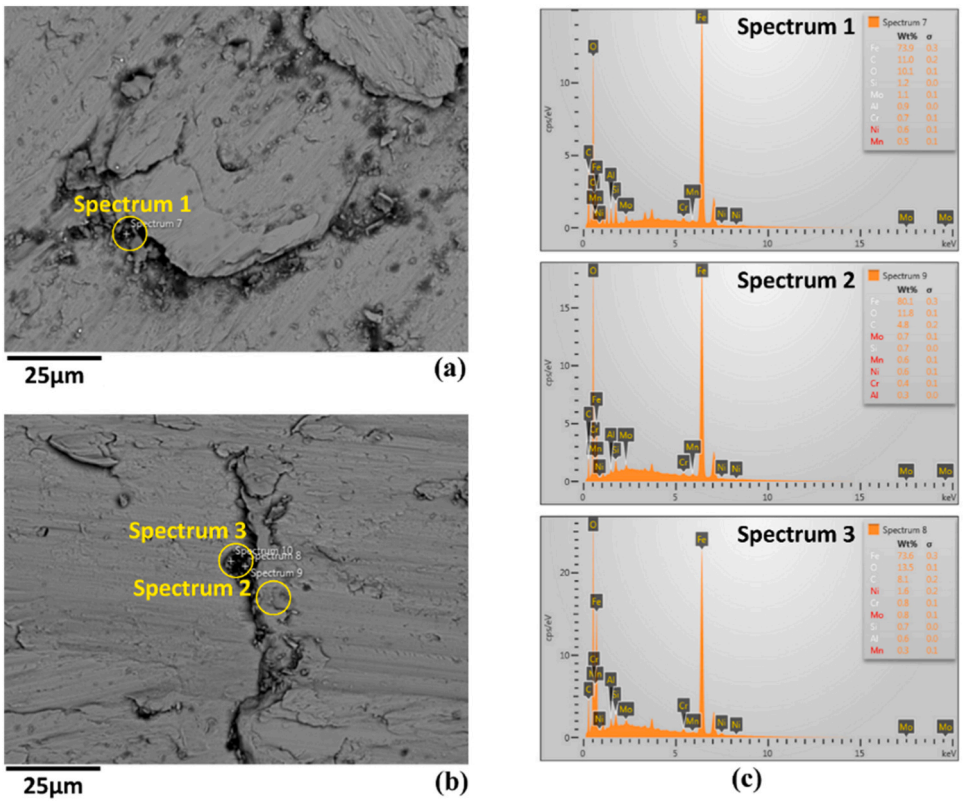

Fig. 21. SEM image from intermixing particles that formed at surface of (a) Case (V) and (b) Case (VI). (c) EDS point analysis from area 1, 2 and 3.

combination of the pin and disk alloy elements and the high amount of oxygen.

4.8. Wear mechanism of Disk

The SEM images from the surface of Case (I) and Case (V) that depicted in Fig. 22a and 22b, reveal distinctive tribological characteristics in the hot pin-on-disk tribo-test.

In Case (I), characterized by a lower normal load of 1 N, the surface exhibits signs of cutting and abrasive wear. The accompanying BSE image illustrates flattening, suggesting plastic deformation of the Super Cr13 steel disk. The hardness disparity between the pin (1.2740 steel)

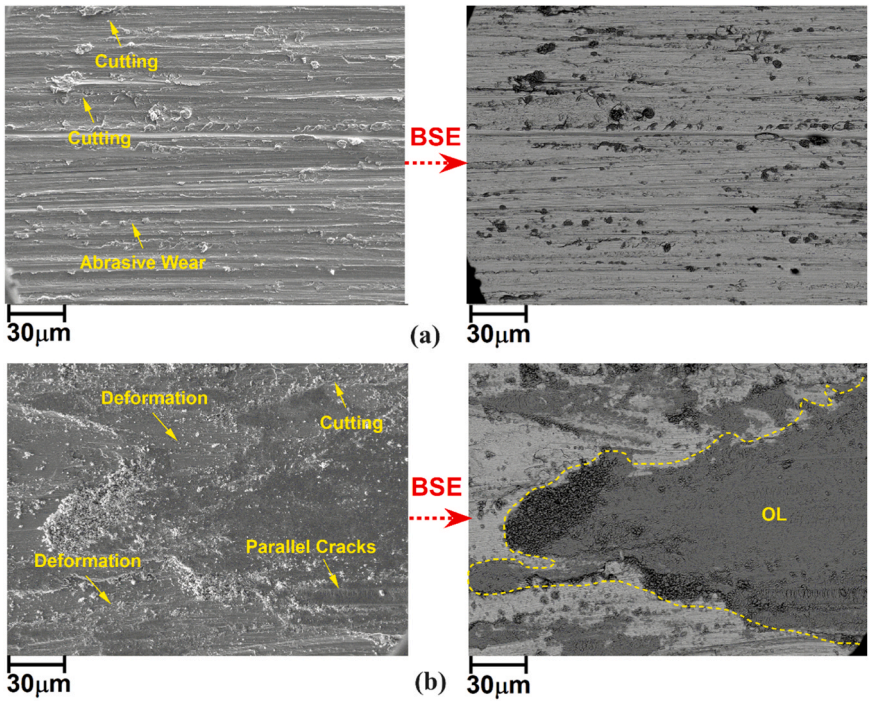

Fig. 22. SE and BSE images from surface of disk in (a) Case (I) and (b) Case (V).

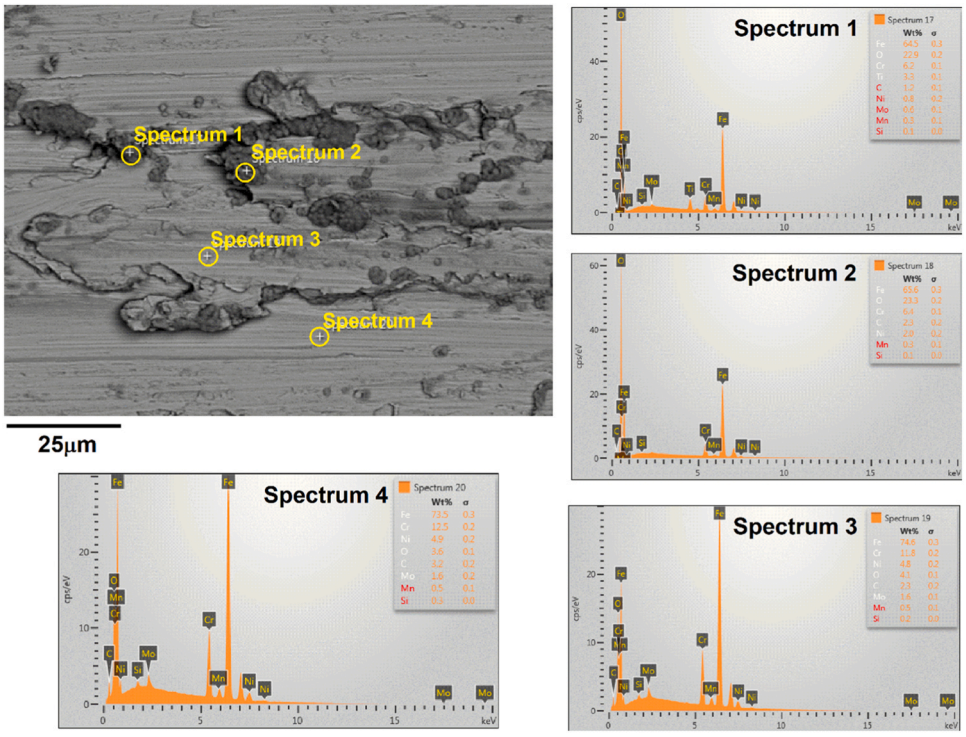

Fig. 23. SEM image from intermixing particles that formed at disk surface of Case (V).

and the disk (Super Cr13 steel) contributes to the observed plastic deformation on the softer disk surface. Conversely, in Case (V), subjected to a higher normal load of 10 N, the disk surface displays more pronounced plastic deformation, with evident cutting and parallel cracks. A substantial oxide layer is detected on the disk's surface, hinting at potential oxidation phenomena. This oxide layer may originate from the disk's surface or, alternatively, result from adherence between the pin and disk surfaces under the elevated normal loads. The substantial plastic deformation and oxide layer formation underscore the complex interplay of mechanical and chemical factors in the tribological behavior, shedding light on the nuanced dynamics within the pin-on-disk system under varying loading conditions [25]. The presence of intermixing zones on the disk surface is evident upon investigation, with their occurrence becoming more pronounced as the normal loads increase (Fig. 23). In particular, the surface analysis of Case (V), depicted through SEM imaging and EDS analysis in Fig. 23, provides insights into

the composition of these intermixing zones. The EDS spectra obtained from these regions reveal a composition comprising elements from both the disk and pin materials. The intensification of intermixing zones with elevated normal loads suggests a more intricate interaction between the tool steel pin and the Super Cr13 steel disk. The intermixing phenomenon may result from enhanced plastic deformation, adhesion, or material transfer under higher loads. The SEM image and corresponding EDS analysis of Case (V) collectively emphasize the dynamic nature of the tribological processes, showcasing not only the physical changes on the disk surface but also the chemical interplay between the contacting materials.

5. Conclusions

In this study, a hot pin-on-disk test was conducted at 700 °C to evaluate the wear and friction properties of DIN 1.2740 hot working tool steel against Super Cr13 MSS under various sliding velocities and normal loads. The results provide valuable insights into the tribological behaviour of the tested steels and highlight important factors influencing their performance at high temperatures, as listed below:

1. The coefficient of friction (COF) between the tested metals exhibited a range of 0.15-0.61. Notably, the COF showed higher stability at high normal loads and low sliding velocities. This indicates that higher loads and lower velocities promote frictional behaviour and reduce fluctuations in the COF.
2. The surface analysis of the DIN 1.2740 disk revealed the presence of a complex oxide layer mixed with deformation layers. The oxide layer exhibited a significant amount of oxygen, along with elements from the pin such as Si, Ni, Cr, and Mo. This complex oxide layer formed during the test contributed to the reduction in COF. However, the fragile nature of the oxide layer at high normal loads and low sliding velocities led to its fracture, resulting in non-uniform surface roughness.
3. The main wear mechanism observed during the pin-on-disk testing of DIN 1.2740 against Super Cr13 MSS at high temperature was abrasive wear, accompanied by deformation of the oxide layer. Additionally, the presence of deformation bands and intermixing particles contributed to ploughing and cutting, leading to further damage of the pin.
4. The Super Cr13 steel (Disk material) tolerated more plastic deformation compare to DIN 1.2740 steel (Pin material). The cutting and abrasive wear detected on the surface of Disks. The oxide layer covers the surface of disk and intermixing zones detected on the disk surface.

CRediT authorship contribution statement

Hamed Aghajani Derazkola: Writing – review & editing, Writing – original draft, Visualization, Validation, Supervision, Resources, Project administration, Methodology, Investigation, Formal analysis, Data curation, Conceptualization. **Dieter Fauconnier:** Writing – original draft, Visualization, Validation, Formal analysis. **Ádám Kalácska:** Writing – original draft, Visualization, Validation, Methodology. **Eduardo Garcia:** Writing – original draft. **Alberto Murillo-Marrodán:** Writing – original draft. **Patrick De Baets:** Writing – review & editing, Writing – original draft, Visualization, Project administration, Funding acquisition, Formal analysis, Data curation.

Declaration of Competing Interest

The authors declare that they have no known competing financial interests or personal relationships that could have appeared to influence the work reported in this paper.

Data Availability

Data will be made available on request.

References

[1] Decrozant-Triquenaux J, Pelcastre L, Courbon C, Prakash B, Hardell J. Effect of surface engineered tool steel and lubrication on aluminium transfer at high temperature. Wear 2021;477:203879. https://doi.org/10.1016/j.wear.2021.203879.

[2] Pelcastre L, Kurnia E, Hardell J, Decrozant-Triquenaux J, Prakash B. High temperature tribological studies on hardfaced tool steels for press hardening of Al-Si coated boron steel. Wear 2021;476:203728. https://doi.org/10.1016/j.wear.2021.203728.

[3] LI S, XU J, YIN Y, XUE J, FENG Y. Mechanism of internal surface crack formation of seamless modified 9Cr-1Mo steel tube rolled by mandrel mill and its application. J Iron Steel Res, Int 2007;14:273–6. https://doi.org/10.1016/S1006-706X(08)60093-X.

[4] Vargas JM, Pagliano C, Medina F, Muratori F, Paganin F, Paiuk J. Process optimization for the manufacturing of seamless steel tubes in a continuous mandrel mill and a stretch reducing mill. IFAC Proc Vol 1989;22:147–53. https://doi.org/10.1016/S1474-6670(17)53102-X.

[5] Gasem ZM. Cracking in a multiple gas-nitrided H13 aluminum extrusion mandrel. Eng Fail Anal 2013;31:68–75. https://doi.org/10.1016/j.engfailanal.2013.01.014.

[6] Skela B, Sedlaček M, Kafexhiu F, Podgornik B. Influence of microstructure and mechanical properties of hot-work tool steel on wear resistance subjected to high-stress wear conditions. Tribol Lett 2020;68:58. https://doi.org/10.1007/s11249-020-01300-1.

[7] Podgornik B, Žužek B, Kafexhiu F, Leskovšek V. Effect of Si content on wear performance of hot work tool steel. Tribol Lett 2016;63:5. https://doi.org/10.1007/s11249-016-0695-6.

[8] Tian X, Zhang Y, Li J. Investigation on tribological behavior of advanced high strength steels: influence of hot stamping process parameters. Tribol Lett 2012;45:489–95. https://doi.org/10.1007/s11249-011-9908-1.

[9] Xianhua C, Qianqian S, Ju W. High temperature wear characteristics of a new hot work die steel CH95. J Wuhan Univ Technol-Mater Sci Ed 2006;21:7–11. https://doi.org/10.1007/BF02840867.

[10] Wei M, Wang S, Wang L, Chen K. Effect of microstructures on elevated-temperature wear resistance of a hot working die steel. J Iron Steel Res Int 2011;18:47–53. https://doi.org/10.1016/S1006-706X(12)60021-1.

[11] ⟨https://www.tubosreunidosgroup.com/en/home⟩ n.d.

[12] Maculotti G, Goti E, Genta G, Mazza L, Galetto M. Uncertainty-based comparison of conventional and surface topography-based methods for wear volume evaluation in pin-on-disc tribological test. Tribol Int 2022;165:107260. https://doi.org/10.1016/j.triboint.2021.107260.

[13] Jayashree P, Candeo S, Matějka V, Foniok K, Leonardi M, Straffelini G. Study on the effect of the addition of bulk and exfoliated graphitic carbon nitride on the dry sliding behavior of a commercial friction material formulation through pin on disc and subscale dynamometer analysis. Tribol Int 2023;179:108152. https://doi.org/10.1016/j.triboint.2022.108152.

[14] Xu X, van der Zwaag S, Xu W. Prediction of the abrasion resistance of construction steels on the basis of the subsurface deformation layer in a multi-pass dual-indenter scratch test. Wear 2015;338–339:47–53. https://doi.org/10.1016/j.wear.2015.05.012.

[15] Banerji A, Lukitsch MJ, McClory B, White DR, Alpas AT. Effect of iron oxides on sliding friction of thermally sprayed 1010 steel coated cylinder bores. Wear 2017;376–377:858–68. https://doi.org/10.1016/j.wear.2017.02.032.

[16] Zhu Y, Chen X, Wang W, Yang H. A study on iron oxides and surface roughness in dry and wet wheel−rail contacts. Wear 2015;328–329:241–8. https://doi.org/10.1016/j.wear.2015.02.025.

[17] De Oliveira MM, Costa HL, Silva WM, De Mello JDB. Effect of iron oxide debris on the reciprocating sliding wear of tool steels. Wear 2019;426–427:1065–75. https://doi.org/10.1016/j.wear.2018.12.047.

[18] Ta TD, Kiet Tieu A, Tran BH. Influences of iron and iron oxides on ultra-thin carbon-based tribofilm lubrication. Tribol Int 2022;173:107665. https://doi.org/10.1016/j.triboint.2022.107665.

[19] Cruz MR, Staia MH. Ion nitrided AISI H13 tool steel Part 2 – High temperature performance under sliding wear conditions. Surf Eng 2007;23:223–9. https://doi.org/10.1179/174329407×174443.

[20] Buscail H, Josse-Courty C, Jacob YP, Le Coze J. Effect of coating on oxidation of impure (C,Mn) iron at 700°c: yttrium–impurity interactions. Surf Eng 2000;16:23–30. https://doi.org/10.1179/026708400322911474.

[21] Dohda K, Boher C, Rezai-Aria F, Mahayotsanun N. Tribology in metal forming at elevated temperatures. Friction 2015;3:1–27. https://doi.org/10.1007/s40544-015-0077-3.

[22] Dohda K, Yamamoto M, Hu C, Dubar L, Ehmann KF. Galling phenomena in metal forming. Friction 2021;9:665–85. https://doi.org/10.1007/s40544-020-0430-z.

[23] Markov DP. Adhesion at friction and wear. Friction 2022;10:1859–78. https://doi.org/10.1007/s40544-021-0564-7.
[24] Macêdo G, Pelcastre L, Hardell J. High temperature friction and wear of post-machined additively manufactured tool steel during sliding against AlSi-coated boron steel. Wear 2023;523:204753. https://doi.org/10.1016/j.wear.2023.204753.
[25] Pujante J, Vilaseca M, Casellas D, Riera MD. The role of adhesive forces and mechanical interaction on material transfer in hot forming of aluminium. Tribol Lett 2015;59:10. https://doi.org/10.1007/s11249-015-0542-1.